THE ASTROPHYSICAL JOURNAL, 325:49–73, 1988 February 1

THE MORPHOLOGY OF MULTIPLE-NUCLEUS BRIGHTEST CLUSTER GALAXIES

TOD R. LAUER
Princeton University Observatory
Received 1987 March 31; accepted 1987 July 28

ABSTRACT

The morphology of 16 multiple-nucleus brightest cluster galaxies has been analyzed by modeling CCD images of the systems as line-of-sight superpositions of normal "secondary" cluster galaxies seen against a brighter "primary" galaxy. Fifty percent of the systems show morphological disturbances not seen in isolated elliptical galaxies and are thus assumed to be galaxies in tidal contact. Interaction effects include asymmetrical isophote distortions of the components, truncated brightness profiles of the secondaries, distended brightness profiles in the inner regions ($r \lesssim 20$ kpc) of the primaries, and the presence of faint plumes that may be dynamical friction wakes. The remaining 50% of the systems are morphologically consistent with superposition of undisturbed galaxies; their components are assumed not to be in tidal contact. No dynamical differences between interacting and noninteracting systems are apparent—interaction effects are found between components with large velocity differences ($\Delta V > 1000$ km s^{-1}), which will lead to tidal stripping of the secondaries involved, as well as those more compatible with merging of the secondaries with the primaries ($\Delta V < 300$ km s^{-1}). The average integrated luminosity of secondaries projected within the metric radius ($r = 10h^{-1}$ kpc) is $0.79L^*$ for the entire sample; of this total the estimated luminosity of secondaries now being cannibalized is $0.17L^*$ per primary. When averaged over all Abell clusters, this result leads to an estimated cannibalism rate of $L_T \approx 2L^*$ per 5×10^9 yr for the brightest cluster galaxy. This in turn implies a dynamical correction of $\Delta q_0 \approx 0.3$ to q_0 measured from metric luminosities of brightest cluster galaxies.

Subject headings: galaxies: clustering — galaxies: evolution — galaxies: photometry

I. INTRODUCTION

It is commonly believed that growth of first-ranked galaxies, if not their formation, depends on some amount of cannibalization of other cluster galaxies (Ostriker and Tremaine 1975; Hausman and Ostriker 1978). Hausman and Ostriker (1978) in particular draw attention to the numerous "nuclei" seen in association with first-ranked galaxies, which they suggest may be the remains of less luminous galaxies being absorbed by them. This idea is compelling and is often discussed as the most striking result of cannibalism, but the relationship between multiple-nucleus systems and galactic cannibalism remains an unsolved problem. Between 28% and 45% of first-ranked galaxies in Abell clusters have more than one "secondary" nucleus within a metric radius ($r = 10h^{-1}$ kpc) of their centers (Hoessel 1980; Schneider, Gunn, and Hoessel 1983*a*). This level of multiplicity is nearly an order of magnitude larger than that expected for chance line-of-sight superpositions of galaxies within the isothermal core of a rich cluster (Tonry 1984). Schneider, Gunn, and Hoessel (1983*a*) further show that multiplicity has little to do with cluster richness and is peculiar to the brightest galaxy—the second- and third-ranked galaxies are rarely multiple. These results suggest some process that brings cluster galaxies into apparent contact with the first-ranked galaxy; however, dynamical observations show that all secondaries cannot now be merging with their primaries. Jenner (1974), Tonry (1984, 1985*a*), and Smith *et al.* (1985) all have shown that the secondaries generally have radial velocities relative to their primaries inconsistent with circular orbits bound to the primary (Tonry 1984); as discussed in § V, the velocity distribution of the secondaries is accurately Gaussian and consistent with them being drawn from the high-dispersion (typically ~ 1000 km s^{-1}) cluster core population. Tonry (1984, 1985*b*) argues that the secondaries are on elongated radial orbits that would explain their large radial velocities and apparent projection against a bright galaxy located at the cluster center. Beers and Tonry (1986) further show that rich galaxy clusters do not have flat cores, but have power-law distributions of galaxies even into their centers; this would also lead to apparent density enhancements of galaxies around one already centrally located. Merritt (1984) considers the strength of dynamical friction in clusters and argues for only mild orbital evolution within cluster cores. Galaxies would be drawn in to the center enough to create central density enhancements with the observed hot dynamics, but strong cannibalism would not take place. Merritt (1985) concludes that a central galaxy in a rich cluster would be expected to grow by only $\sim 1L^*$ over the cluster lifetime as compared to the typical brightness $\sim 12L^*$ of the first-ranked galaxy.

The key question is to what extent multiple systems are composed of galaxies in physical contact as opposed to chance line-of-sight superpositions of galaxies within the core of a cluster. This paper attempts to answer this question directly by morphological analysis of 16 multiple-nucleus first-ranked galaxies in Abell clusters. The principal tool used is a multiple-isophote decomposition algorithm that models CCD images of the systems under the hypothesis that they can be described by simple superposition of galaxies with concentric elliptical isophotes (Lauer 1986), which is a highly accurate description of isolated elliptical galaxies (Lauer 1985). Surface photometry profiles are derived simultaneously for all components in the systems and can be compared to those of normal galaxies. Further, models of any component can be subtacted from the images to uncover subtle morphological distortions of the galaxies that might imply mutual tidal interaction. The decomposition algorithm was applied initially to the classic multiple-nucleus cD galaxy in A2199; evidence was found suggestive of deep interpenetrating high-speed encounters by its secondaries (Lauer 1986). The systems analyzed here exhibit a wealth of interaction effects and show that, in many cases, multiple systems are interacting systems.

II. OBSERVATIONS AND DECOMPOSITION

a) The Sample

The sample of multiple first-ranked galaxies presented here (see Table 1) is drawn from the list of multiple systems identified by Hoessel (1980) in a complete survey of first-ranked galaxies in Abell clusters. Hoessel's criterion for classification of a system as multiple is the presence of one or more secondary galaxies within one metric radius ($10h^{-1}$ kpc) of the first-ranked galaxy's nucleus. Although this definition is somewhat arbitrary, it draws attention to systems whose components would be strongly affected by mutual tidal interactions if the components' physical separations were similar to their projected values. Otherwise, Hoessel's catalog of multiple systems should not contain any biases toward clusters where *present* physical interaction of the central galaxies is expected on other grounds. Table 1 gives the Rood-Sastry (Struble and Rood 1982) and Bautz-Morgan (Leir and van den Bergh 1977) classifications of the Abell clusters to describe qualitatively their overall structure and the prominence of their first-ranked galaxies. As can be seen, only six of the first-ranked galaxies are true cD galaxies; the remaining first-ranked galaxies appear to be giant ellipticals, as elaborated in § III. Table 1 also presents cluster redshifts taken from Hoessel (1980), with revised values for A1291 and A1927 given by Smith *et al.* (1985), and where available, cluster velocity dispersions from Struble and Rood (1987).

b) Observations and Reduction

Images of most of the multiple systems were kindly obtained by J. E. Gunn, using the 4-Shooter CCD camera (Gunn *et al.* 1987) mounted at the Cassegrain focus of the Hale 5 m reflector. For the present study, which concentrates on the central galaxy in the Abell clusters, just one of the camera's four CCDs was used. The CCD scale is 0."334 per pixel, which yields a 4.'45 × 4.'45 field. The image of A194 was obtained at Lick Observatory with the 1 m nickel reflector and a TI CCD with a 0."432 scale. Additional Lick images were also available for A400 and A2634. Most of the images were obtained in the *r* band, with the remainder taken in the *g* band. As can be seen in Table 1, exposure times varied between 100 and 500 s—whatever was sufficient to guarantee signal-to-noise ratios in the nuclei of the central galaxies in excess of 100. It should be noted that in the deepest exposures, reflected images of the bright nuclei become visible at position angle 45°; the reflections are always faint, compact, and only become visible when the nuclear exposure level approaches saturation. Seeing was good to excellent for most of the observations and is given in Table 1.

Basic image reduction was carried out with VISTA (Lauer, Stover, and Terndrup 1983) installed under UNIX on Princeton University Observatory's VAX 11/750. Dome flat fields were sufficient to remove CCD sensitivity variations to 2%. Large-scale two-splines fitted to reduced night-sky images were used to reduce these residual variations further to 0.5%. Sky levels were measured in the image corners by standard histogram techniques; for a typical image the sky comes from an area 2.'4 from the nucleus of the first-ranked galaxy in a direction within 45° of its minor axis. For a few of the lower redshift cD galaxies, the sky is contaminated by light from the extended envelope; however, for the present study, this is at most only a minor problem since the photometry is confined to the central 1′ of the galaxies, and as discussed below, uncertainty in the sky level always affects the central bright galaxy rather than the fainter secondary galaxies. Pictures of the final reduced images are presented in Figures 1–16 (Plates 1–8). These pictures have been stretched to compress their large dynamic range in surface brightness and have a gray scale "rollover" set to occur at an arbitrary outer isophote to show the alignment of the nuclei of the first-ranked galaxies, which are always centered in the frame, with their envelopes.

TABLE 1

JOURNAL OF OBSERVATIONS

Abell	z	RS Type	BM	σ_{CL} (km s^{-1})	Exposure (s)	Band	Seeing
194.......	0.0178	L	II	435	500	r	1."72
400.......	0.0231	I	II–III	423	200	r	4.55
671.......	0.0497	C	II–III	...	100	r	1.04
779.......	0.0201	cD	I–II	755	200	r	0.84
1126.......	0.0828	B	I–II	...	100	r	1.46
1185.......	0.0349	C	II	785	200	r	1.29
1291.......	0.0512	F	III	975	200	r	1.05
1468.......	0.0853	C	I	...	300	r	1.30
1496.......	0.0961	I	III	...	300	r	1.01
1656.......	0.0230	B	II	880	300	r	1.32
1927.......	0.0972	cD	I–II	...	300	r	1.54
1991.......	0.0589	cD	I	...	300	g	1.48
2052.......	0.0351	cD	I–II	570	300	r	1.96
2063.......	0.0337	cD	II	521	300	g	1.76
2151.......	0.0360	F	III	887	300	g	1.63
2634.......	0.0315	cD	II	899	200	r	3.61

c) Decomposition of the Multiple Systems

Surface photometry profiles are measured for all component galaxies in the multiple systems by a multiisophote decomposition algorithm developed by Lauer (1986). The decomposition algorithm is summarized here briefly; the reader is referred to Lauer (1986) for further details. Basically it is assumed that each system can be modeled as the line-of-sight superposition of one or more normal elliptical galaxies against a central cD or giant elliptical. The structure of each galaxy is thus assumed to be well described by a set of concentric elliptical isophotes with otherwise arbitrary surface brightness, position angle, and ellipticity profiles as a function of isophote semimajor axis length. The modeled intensity at any pixel in the image is found by adding the contribution from each galaxy, which is estimated by interpolation between its isophotes. The isophote parameters are estimated initially by fitting simple harmonic functions to the image and then are revised by an iterative nonlinear least-squares algorithm that minimizes differences between the modeled and observed pixel values.

The success at modeling any multiple system as simple superposition of normal galaxies can be tested directly by examining the residuals of the model fit; failures of the decomposition are always interesting and reveal evidence for interaction between galaxies in the systems. Once the isophote parameters have been measured, any or all of the component galaxies can be subtracted from the observed image; asymmetrical distortions of the isophotes, tidal tails, or any other features not described by the model become readily visible. In general, the decomposition algorithm can uncover deviations from the superposition model down to levels of only a few

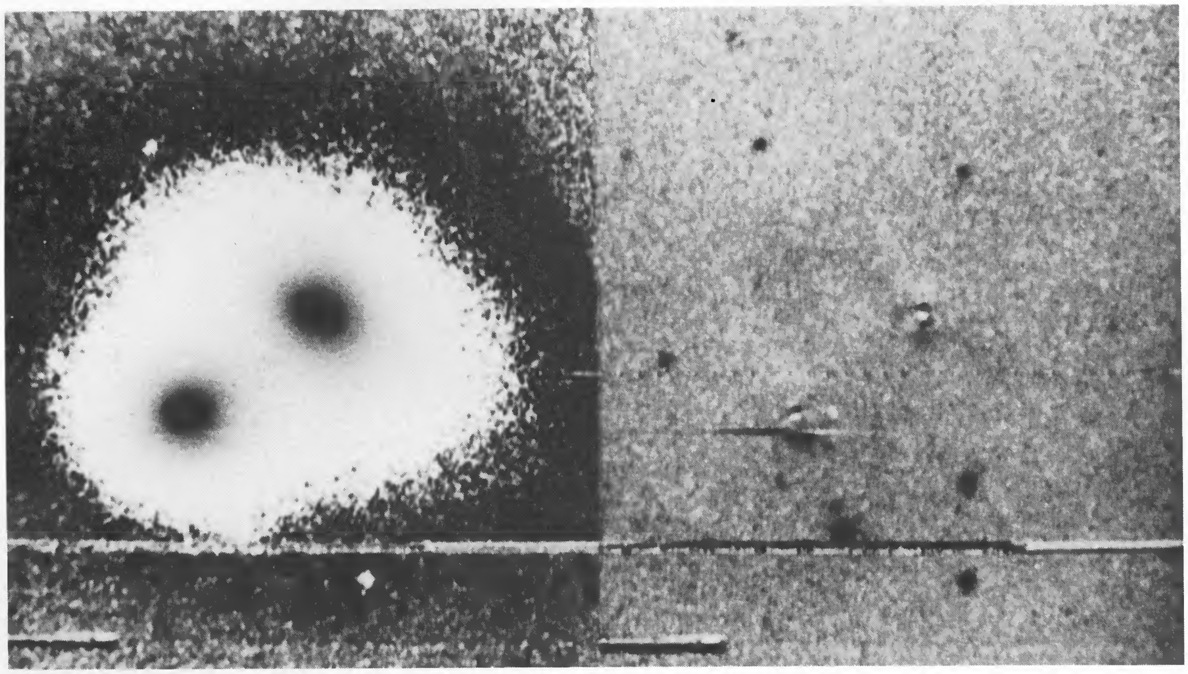

FIG. 1.—CCD image of the multiple system in A194 (*left panel*) and the residual map of the decomposition algorithm model fit (*right panel*). Each panel is 121″ on a side. In this and all subsequent figures, the image in the left panel has been stretched logarithmically to compress its dynamic range, and a gray-scale "rollover" has been set to occur at an arbitrary outer isophote. The residual map has been normalized by the expected shot-noise residuals; $+5\ \sigma$ residuals are black, and $-5\ \sigma$ residuals are white. The primary galaxy is centered on both panels. North is at the top. Note the flatness of the residual map.

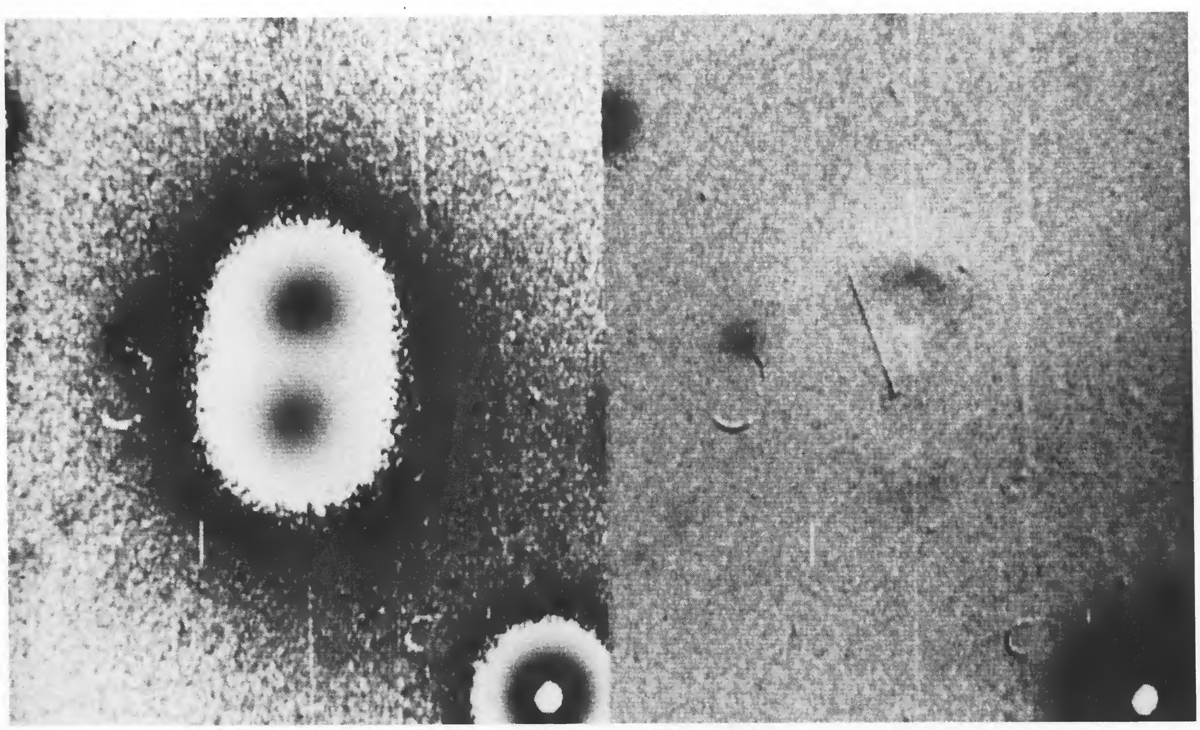

FIG. 2.—CCD image and residual map of the A400 system as in Fig. 1. Each panel is 100″ on a side. Note the arclike patterns in the residual map, showing that A400A has nonconcentric isophotes.

1988ApJ...325...49L

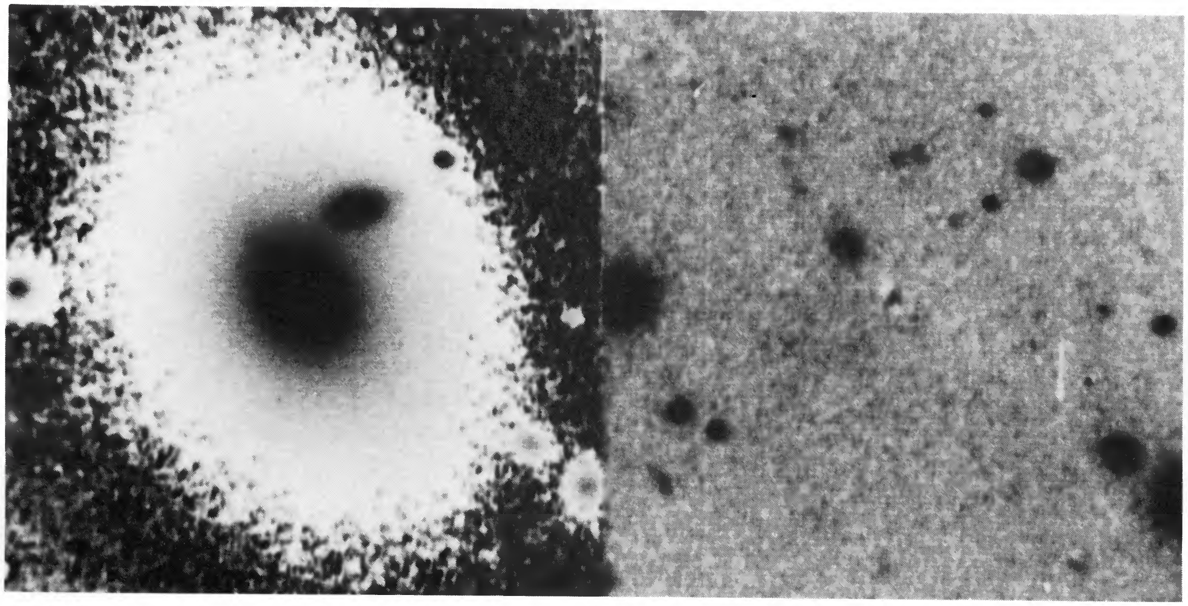

FIG. 3.—CCD image and residual map of the A671 system as in Fig. 1. Each panel is 67″ on a side. Note the flatness of the residual map.

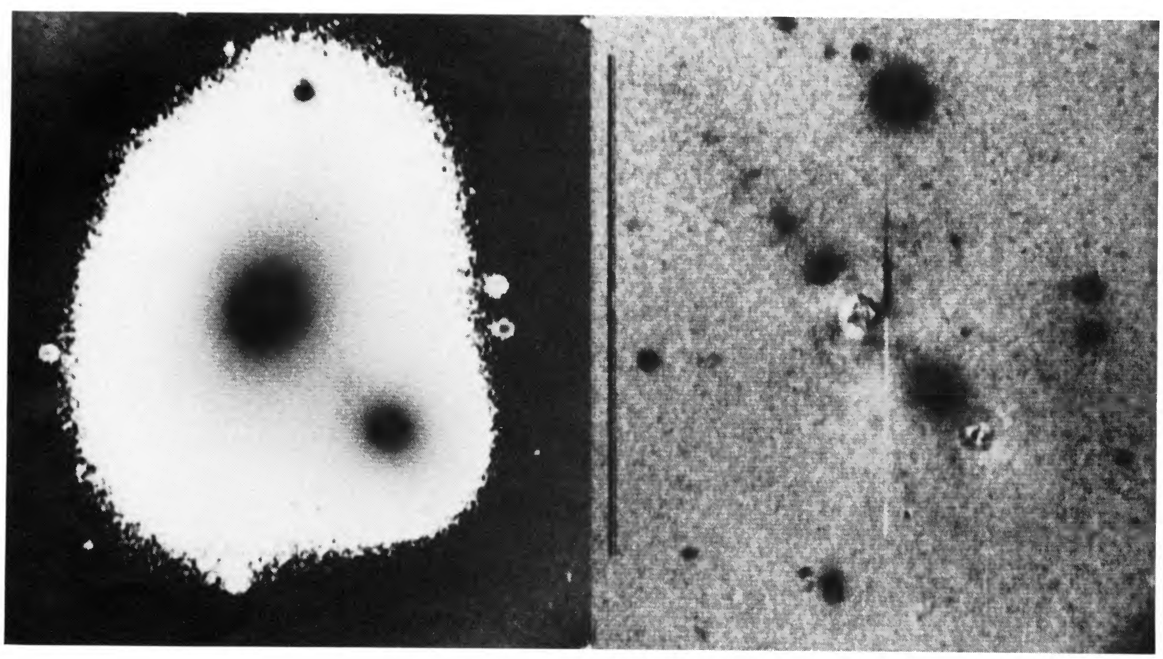

FIG. 4.—CCD image and residual map of the A779 system as in Fig. 1. Each panel is 94″ on a side. The faint compact features to the NW of A779A are reflections of its nucleus; the suspected dynamical friction wake associated with A779B, the diffuse feature between A779A and A779B, is stronger and more extended than the reflections. Differential truncation of A779B is suggested by the arc of negative residuals visible to its NW. The nuclei of both A779A and A779B were overexposed and were filled in from shorter exposures.

LAUER (*see* **325**, 50)

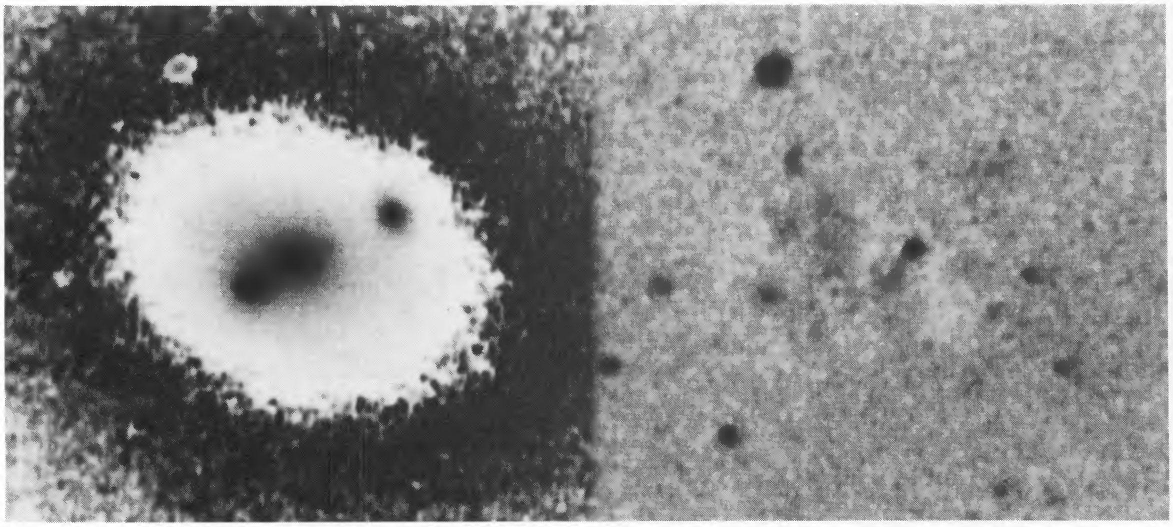

FIG. 5.—CCD image and residual map of the A1126 system as in Fig. 1. Each panel is 53″ on a side. Note the diffuse plumelike patches of emission in the residual map.

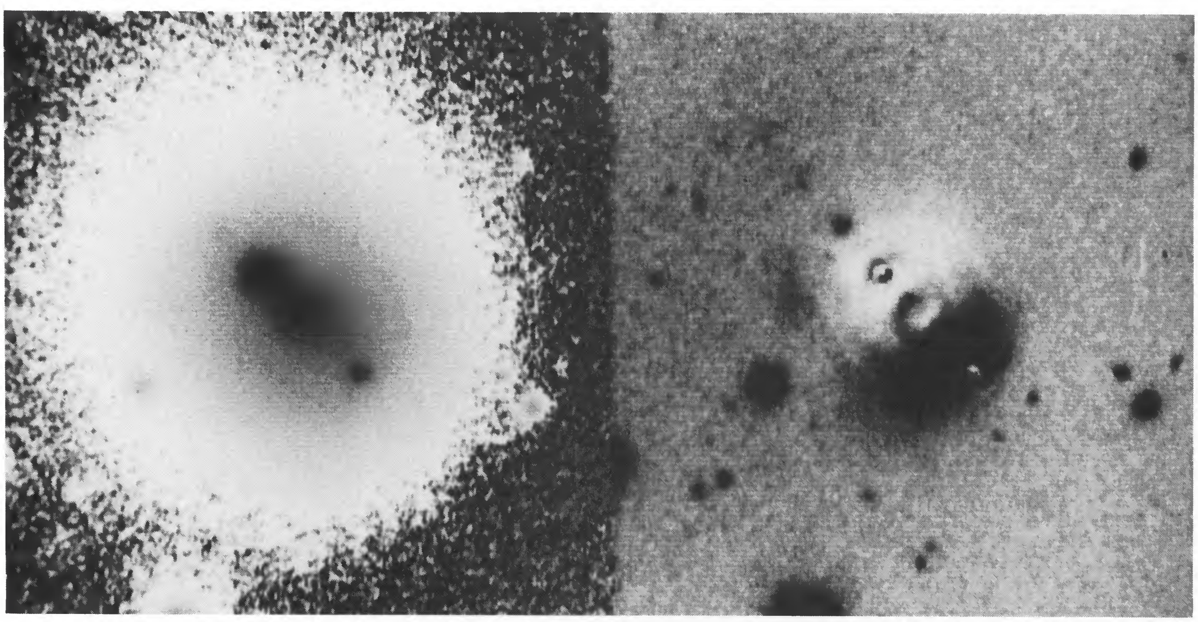

FIG. 6.—CCD image and residual map of the A1185 system as in Fig. 1. Each panel is 86″ on a side. Both panels show the strongly nonconcentric isophotes of A1185A.

LAUER (*see* **325**, 50)

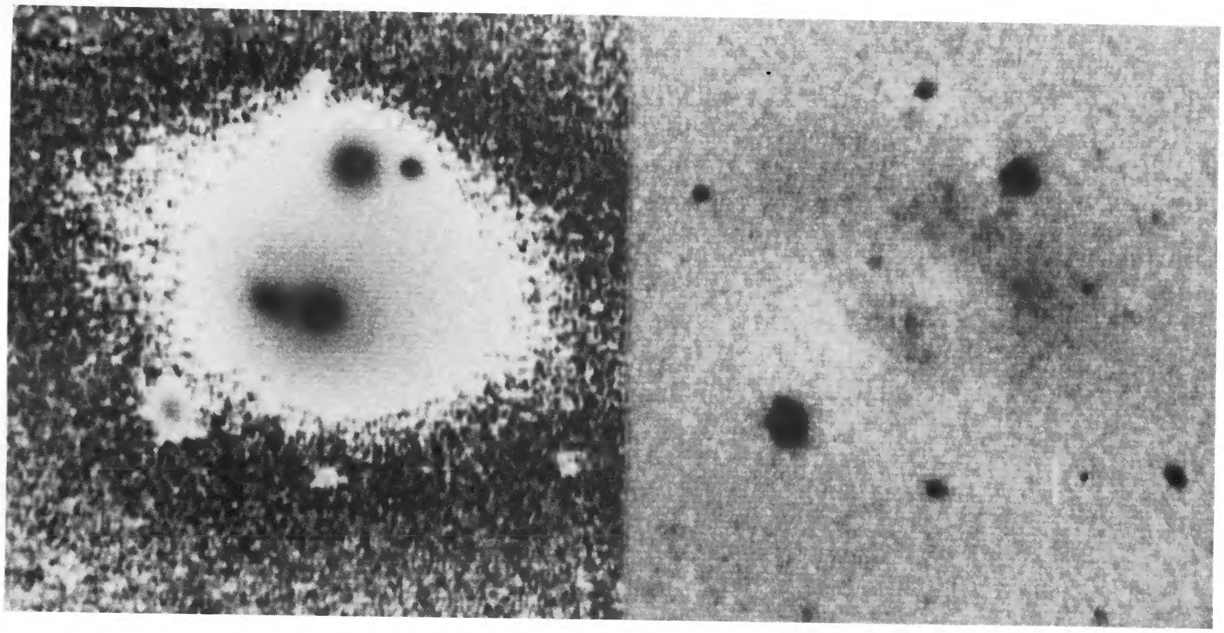

FIG. 7.—CCD image and residual map of the A1291 system as in Fig. 1. Each panel is 67″ on a side. Both panels show the strongly nonconcentric isophotes of A1291A.

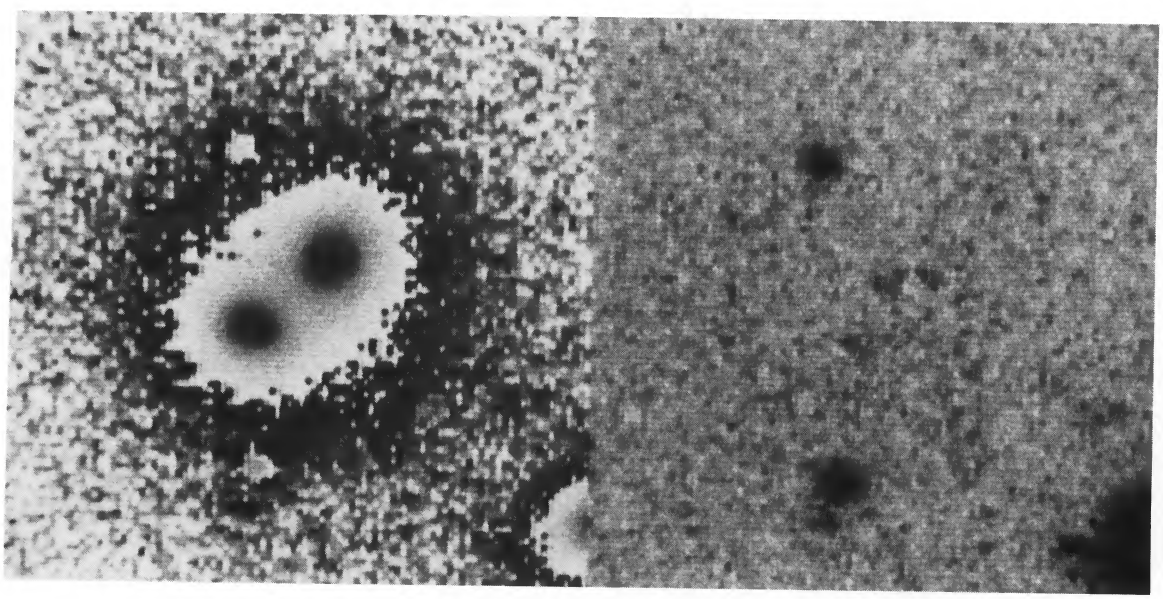

FIG. 8.—CCD image and residual map of the A1468 system as in Fig. 1. Each panel is 33″ on a side. Note the flatness of the residual map.

LAUER (*see* **325**, 50)

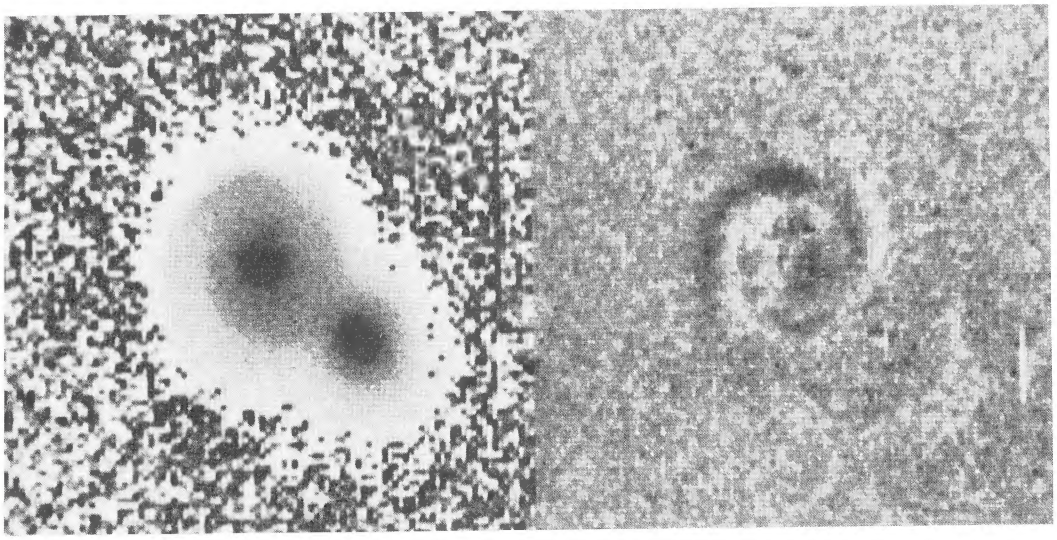

FIG. 9.—CCD image and residual map of the A1496 system as in Fig. 1. Each panel is 33″ on a side. Note the spiral-like patterns in the residual map around A1496A.

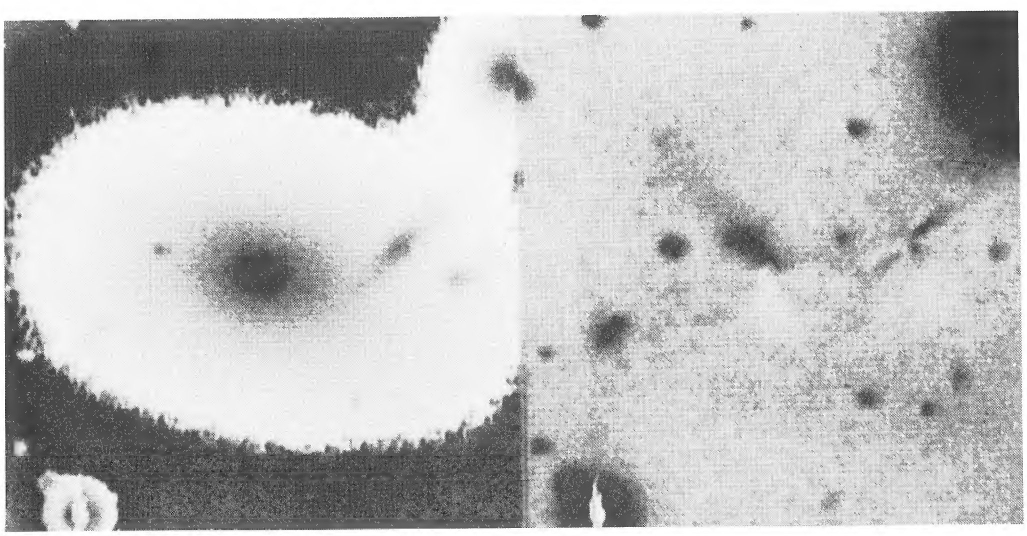

FIG. 10.—CCD image and residual map of the A1656 system as in Fig. 1. Each panel is 100″ on a side. The residual image is flat, but for reflections of A1656A's nucleus to the NW, and the disk of A1656B, which was not fitted.

LAUER (*see* 325, 50)

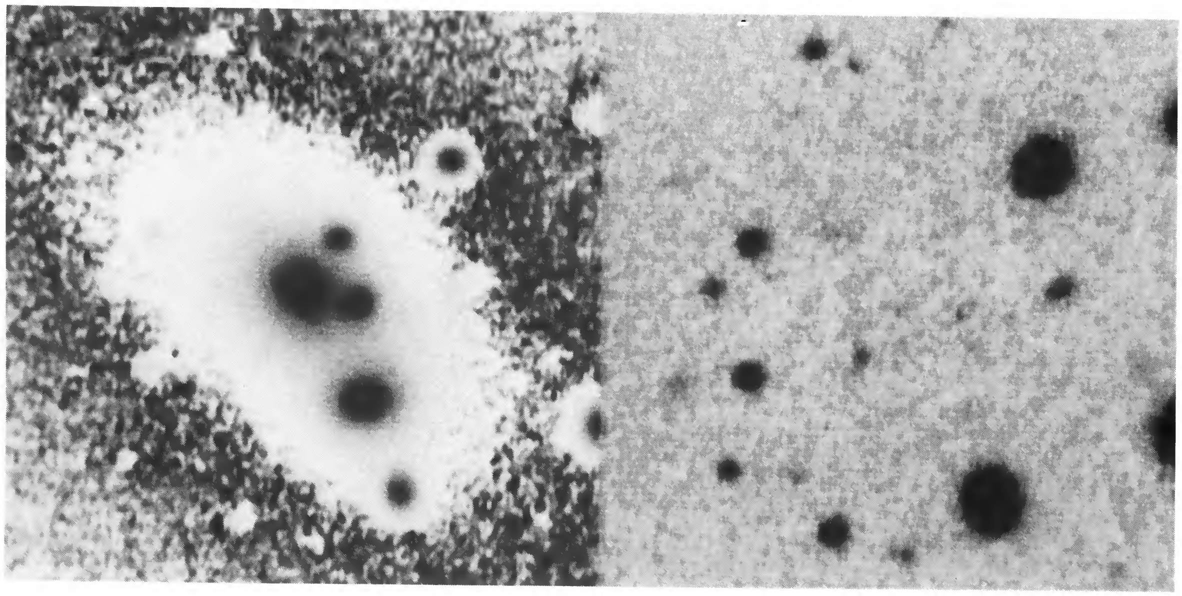

FIG. 11.—CCD image and residual map of the A1927 system as in Fig. 1. Each panel is 60″ on a side. Note the flatness of the residual image.

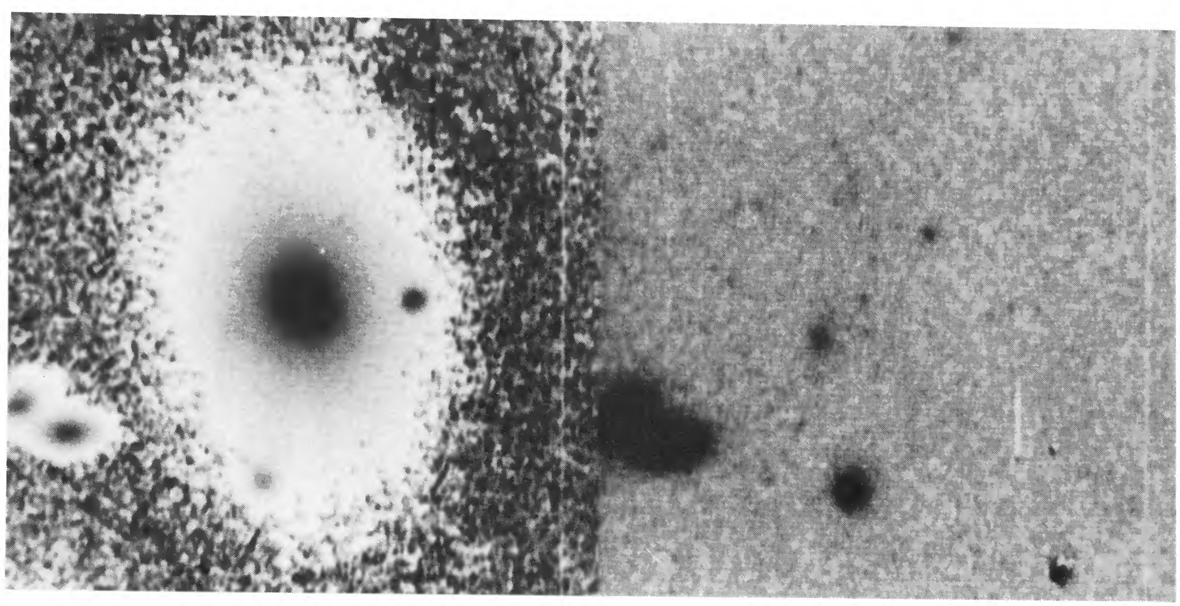

FIG. 12.—CCD image and residual map of the A1991 system as in Fig. 1. Each panel is 67″ on a side. Note the flatness of the residual image.

LAUER (*see* **325**, 50)

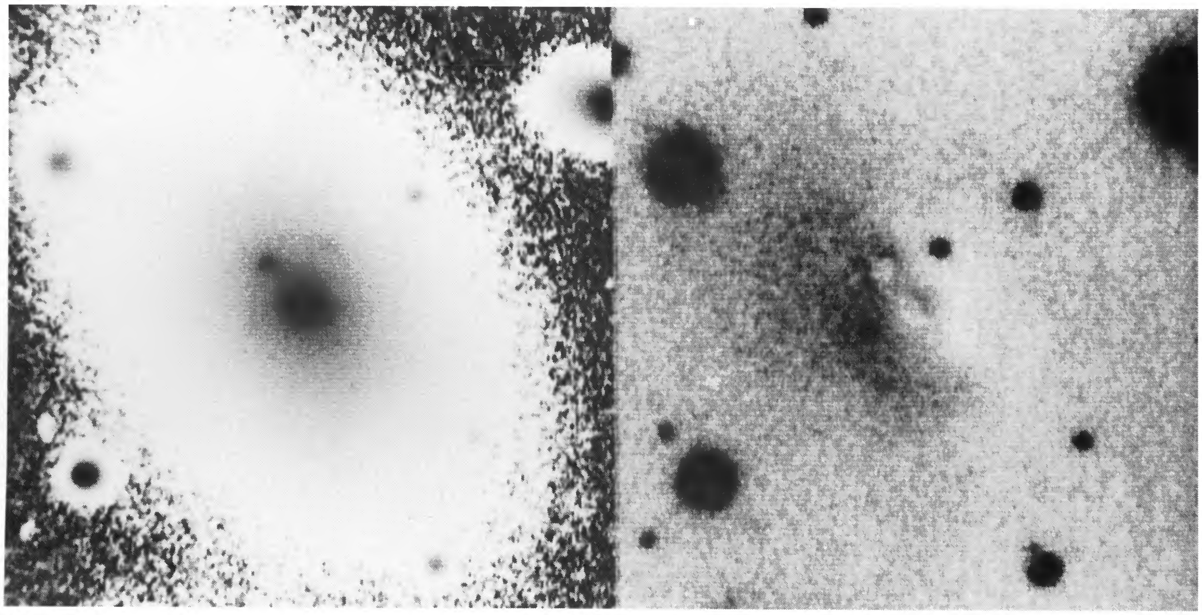

FIG. 13.—CCD image and residual map of the A2052 system as in Fig. 1. Each panel is 86″ on a side. Note the dipole residual pattern associated with A2052A, showing that its nucleus has been displaced from its envelope.

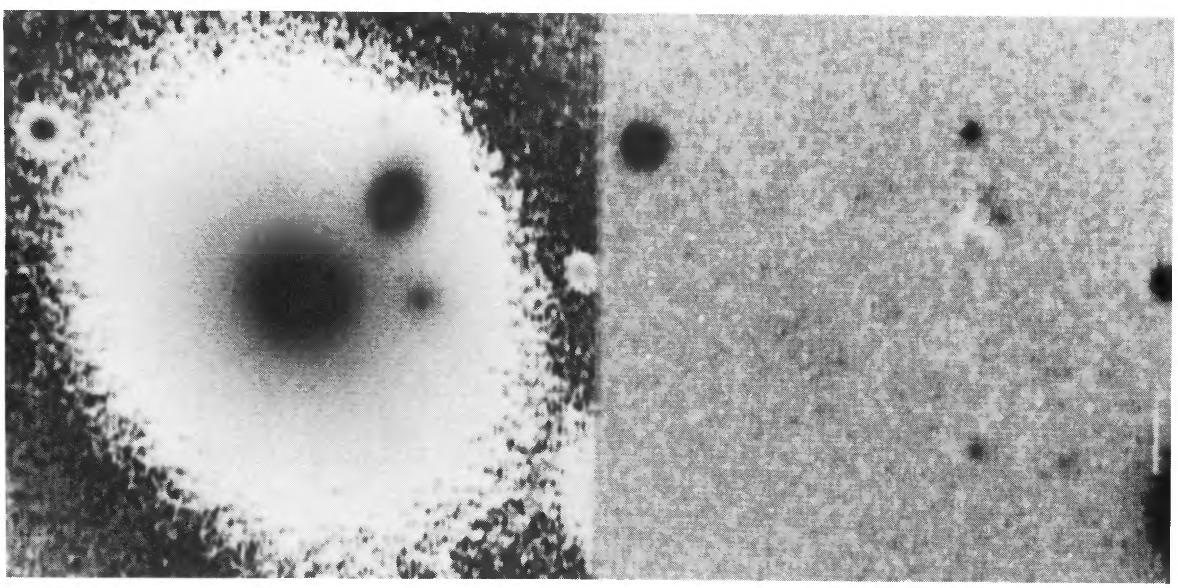

FIG. 14.—CCD image and residual map of the A2063 system as in Fig. 1. Each panel is 67″ on a side. Note the flatness of the residual image.

LAUER (*see* **325**, 50)

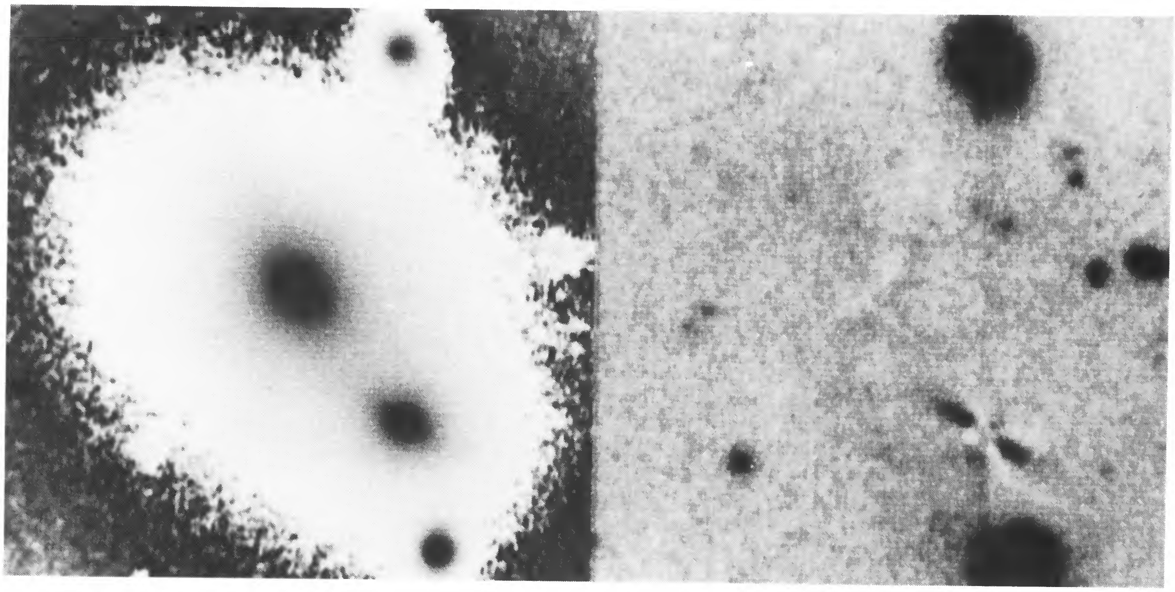

FIG. 15.—CCD image and residual map of the A2151 system as in Fig. 1. Each panel is 67″ on a side. The residual map is flat, but for a weak dust lane associated with the nucleus of A2151A, and the disk associated with A2151B.

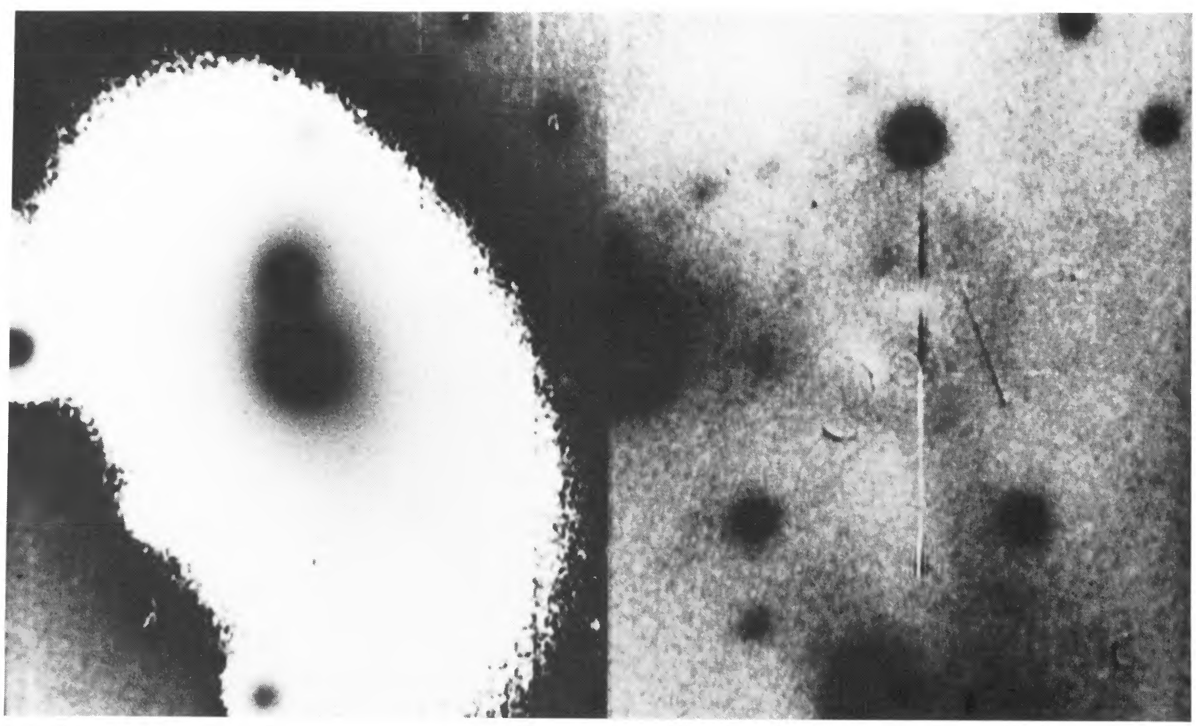

FIG. 16.—CCD image and residual map of the A2634 system as in Fig. 1. Each panel is 100″ on a side. Both panels show the strongly nonconcentric isophotes of A2634A.

LAUER (*see* **325**, 50)

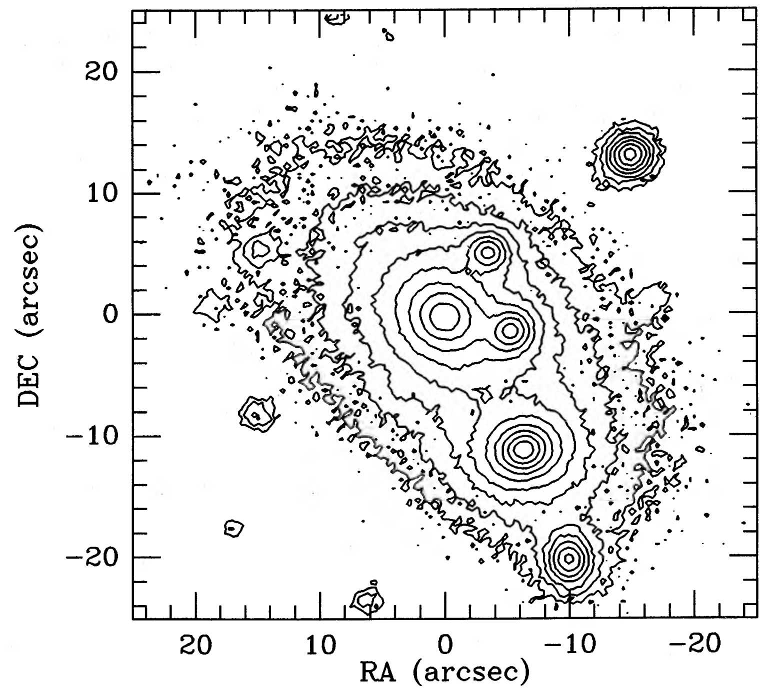

FIG. 17.—Contour map of the multiple system in A1927. Contours are in half-magnitude steps; the outermost contour is at 23.5 mag arcsec^{-2} (*r* band).

percent, given the high signal-to-noise ratio of the images; more specific limits, of course, depend on the specific brightness distributions and exposure levels of the systems being studied. Note, however, that in spite of the pure superposition modeling assumption, the surface photometry algorithm will recover and follow any symmetrical distortion of the isophotes that might result from mutual interaction between the galaxies such as tidally induced isophote stretching or twisting, and truncation or distension of their envelopes.

An example of the composition procedure is presented in Figures 17–19. Figure 17 shows a contour map of the central galaxy A1927, the most complex system in the present study. Figure 18 shows a contour map of the model fit, which included the three nearest secondary galaxies as well as the central galaxy. Figure 19 shows the central galaxy with the fits to the secondary galaxies subtracted. As can be seen, the fits worked well; the isophotes of the central galaxy appear undistorted in the regions strongly dominated in Figure 17 by the secondary galaxies.

In practice, decomposition of any system is done in a few

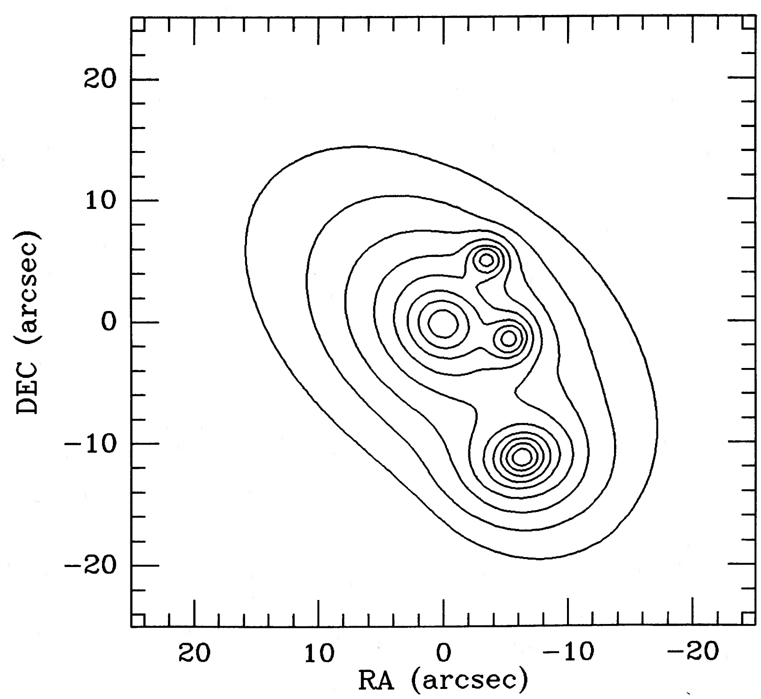

FIG. 18.—Contour map of the model fit to A1927. Contour levels are as in Fig. 17.

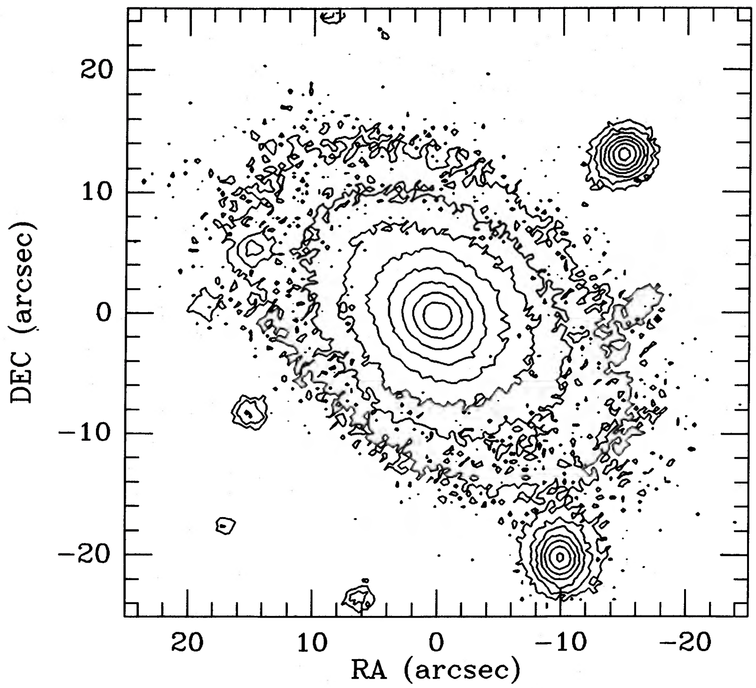

FIG. 19.—Contour map of A1927A alone; models of its three nearest secondary components have been subtracted. Contour levels are as in Fig. 17.

stages. Isophotes are measured for all components at prespecified logarithmically spaced isophote semimajor axis lengths. The isophotes of the brightest galaxy always encompass the other galaxies, so it absorbs any error in the constant sky background. Since a least-squares procedure is used to solve for the isophote parameters, foreground stars, CCD defects, or other localized features such as compact cluster galaxies can be excluded from the fit. This is often done iteratively; low-contrast compact features found in the residual map only after an initial decomposition attempt can be excluded in subsequent iterations.

Table 2 lists all the components fitted in each system. Precise position angles and separations are given for the nuclei of the secondary galaxies relative to the primary nuclei. Note that the nuclei of a few of the secondary galaxies lie outside the metric radius identified above; in all cases these were galaxies that extended well into the metric radius and thus were important for the correct modeling of the systems. Residual maps for all systems are presented in Figures 1–16. All maps have been normalized by the expected shot noise errors and were stretched to the same level; $+5\ \sigma$ residuals are black, and $-5\ \sigma$ residuals are white. Any compact features visible in the maps were excluded from the final isophote fits. The maps are discussed in detail § III*c*.

III. RESULTS

a) *Surface Photometry*

Surface brightness profiles are presented for all multiple-system component galaxies in Figures 20–35. Photometric calibration is provided by the aperture photometry presented by Hoessel (1980); the brightness profiles are left in the original color bands of the observations as listed in Table 1. Error bars shown for the brightness values are calculated based on each isophote's contribution to the χ^2 value of the decomposition residuals. Simulations show that random errors are more important than any systematic errors in the photometry of faint isophotes of secondaries deeply embedded in their primaries; as the results become less significant, the error bars increase to reflect this. Isophote position angle and ellipticity profiles were also calculated for all galaxies, but are not shown, except as warranted by the discussion below, to save space. Tabular presentation of all isophote parameters is available from the author on request.

The surface brightness profiles of the galaxies are plotted as a function of isophote semimajor axis length in arc seconds to the quarter power to permit direct comparison of the profiles with de Vaucouleurs laws, which are straight lines in this coordinate system. This procedure seems to be most useful for understanding the profiles of the secondary galaxies. The profiles of many of the central galaxies seem better described by pure power laws, however, which curve concave-up in the present figures.

b) *Global Parameters*

Luminosities, effective radii, and effective surface brightnesses for all components are presented in Table 2. For convenience, all parameters have been transformed to the B band assuming $B - r = 1.15$ and $B - g = 0.68$ (Schneider, Gunn, and Hoessel 1983*b*). Effective radii and surface brightnesses were measured by fitting a de Vaucouleurs law to the profiles (using the geometric mean of the isophote major and minor axes for the radii of the isophotes) outside the central 3″ to avoid seeing effects. Small R_e values implying angular values less than 3″ for some galaxies simply reflect the steep falloff of their profiles; the R_e values only measure the slope of the profiles. Total apparent magnitudes of the galaxies were calculated from the R_e and I_e values and direct integration of the light within 3″. Absolute magnitudes and all physical scales presented in Table 2 have been calculated assuming $H_0 = 50$ km s^{-1} Mpc^{-1}. The absolute magnitudes are adjusted further

TABLE 2

COMPONENT GALAXY GLOBAL PARAMETERS

Abell	R_{sep} (kpc)	P.A.	m_B	M_B	R_E (kpc)	I_E	$\|\Delta V\|$ (km s^{-1})
194 A	...	...	12.56	−22.66	21	24.00	...
B	14.9	128.0	13.75	−21.47	4.7	21.93	218[a]
400 A	...	...	14.43	−21.46	9.2	23.53	...
B	10.4	355.3	14.54	−21.35	4.6	22.06	426[b]
671 A	...	...	13.98	−23.54	36	24.52	...
B	14.9	329.9	17.80	−19.72	1.2	20.25	655[b]
779 A	...	...	12.60	−22.84	17	23.40	...
B	13.6	225.2	15.16	−20.28	1.9	20.96	1692[b]
1126 A	...	...	14.70	−23.89	54	25.13	...
B	10.6	121.5	18.07	−20.52	1.2	19.12	1299[a]
C	23.0	294.9	18.96	−19.64	1.5	20.83	253[a]
1185 A	...	...	13.60	−23.05	34	24.71	...
B	6.6	43.3	16.62	−20.04	0.33	15.81	57[b]
C	11.0	222.8	18.87	−17.79	0.67	20.57	534[b]
1291 A	...	...	14.75	−22.77	73	26.79	...
B	24.9	346.5	17.33	−20.18	8.7	24.71	...
C	8.0	79.4	19.43	−18.09	0.26	16.93	94[a]
1468 A	...	...	16.55	−22.12	20	24.70	...
B	12.7	132.3	17.99	−20.68	3.1	21.68	12182[a]
1496 A	...	...	17.25	−21.69	11	23.70	...
B	18.4	231.5	18.22	−20.72	4.6	22.72	321[a]
1656 A	...	...	12.43	−23.33	19	23.20	...
B	17.4	280.6	16.36	−19.40	4.4	23.82	1178[a]
C	24.7	268.8	18.10	−17.66	2.4	24.12	...
1927 A	...	...	15.35	−23.61	62	25.78	...
B	30.3	209.9	17.69	−21.27	3.6	21.47	...
C	12.9	256.6	19.26	−19.70	1.1	19.73	...
D	14.9	326.2	20.20	−18.76	0.30	15.88	176[a]
1991	...	...	14.09	−23.87	70	25.74	...
B	19.2	271.5	19.91	−18.05	...	...	...
2052 A	...	...	12.84	−23.86	82	25.87	...
B	6.8	40.7	19.99	−16.72	0.14	15.90	156[b]
2063 A	...	...	13.51	−23.18	49	25.50	...
B	14.1	315.4	17.10	−19.60	0.94	19.72	853[b]
C	12.6	269.0	19.25	−17.45	1.1	22.17	1237[b]
2151 A	...	...	13.83	−22.94	34	24.91	...
B	18.7	219.3	16.38	−20.39	3.5	22.36	786[b]
2634 A	...	...	13.32	−23.19	28	24.20	...
B	10.5	9.1	16.26	−20.25	0.75	18.17	997[b]

NOTE.—Distance-dependent parameters were calculated assuming $H_0 = 50$ km s^{-1} Mpc^{-1}. Radial velocity for the secondaries, where available, are from Tonry 1984, 1985*a* or Smith *et al.* 1985, as noted by note (a) or (b).

for the filter k corrections given by Schneider, Gunn, and Hoessel (1983*b*), and extinction as given in Burstein and Heiles (1984).

c) Remarks on Individual Systems

The major goal of this paper is to uncover any evidence that multiple-nucleus systems might be composed of galaxies in tidal contact; this hypothesis is examined on a case by case basis below. The conclusions reached on whether or not a system contains interacting components and a summary of evidence supporting the conclusions are given in Table 3; the results for A2199, which was analyzed separately (Lauer 1986), are also given in Table 3. Failure of the decomposition algorithm to produce flat residual images due to asymmetric isophote distortions is the best signature of interaction effects; limits on the detectability of distortions are discussed in § IV. The presence of faint features suggestive of tidal plumes or dynamical friction wakes is also taken as an indicator of interaction. Lastly, abnormal component brightness profiles, that is, those that deviate from pure power, exponential, or $r^{1/4}$ laws at more than one isophote by being truncated at large radii or distended at small radii, are also assumed to result from tidal interactions. It must be remembered, however, that success of the superposition assumption for any system cannot disprove but can only constrain the effects of any putative interaction between its components. Further, although clear yes-no decisions are given in the morphology summary presented in Table 3, these often involve more qualitative than quantitative judgement and thus should be regarded as tentative. The most weight has been put on morphological abnormalities not seen in isolated elliptical galaxies. For example, while the decomposition algorithm is able to follow and recover any symmetrical stretching or twisting of the components that might be induced by tidal interactions, since such behavior is often seen in isolated galaxies, it is difficult to argue for interaction on the basis of symmetrical changes in isophote shapes alone.

i) *A194*

This system consists of two galaxies, NGC 545 and NGC 547, of nearly equal luminosity; they do not appear to be interacting. The residual map in Figure 1 is flat; neither tidal features nor any large-scale distortions of the isophotes away are seen. The brightness profile for A194B (NGC 547) appears to follow a normal $r^{1/4}$ law . While the profile for A194A (NGC 545) appears to be distended or puffed up at radii further than 13″ from the nucleus, which may indicate tidal heating (Kormendy 1977), it is also consistent with the classification of NGC 545 as an S0 by de Vaucouleurs, de Vaucouleurs, and Corwin (1976). A weak disk component is visible on sky survey plates, and the brightness profile of NGC 545 plotted in semi-logarithmic coordinates shows that the outer portion of the profile falls off exponentially. Lastly, neither galaxy shows any sign of isophote twisting.

ii) *A400*

This is another binary system with galaxies of nearly equal luminosity. The southern galaxy (A) has lower central surface brightness but higher total luminosity than the northern component (B). A400A appears to have a power-law brightness profile, while A400B follows an $r^{1/4}$ law. The isophotes of galaxy B do not appear to be concentric. The residual map (Fig. 2) shows an arc of positive residuals 5″ north of nucleus B with corresponding negative residuals to the south; at larger radii, this pattern reverses, with an arc of *negative* residuals

TABLE 3

MORPHOLOGY SUMMARY

Abell	Isophote Shear	Primary Excess	Secondary Truncation	Tidal Feature	Interaction
194	...	...	...	...	N
400	×	...	...	...	Y
671	...	...	...	...	N
779	×	...	×	×	Y
1126	...	×	...	×	Y
1185	×	×	...	×	Y
1291	×	×	...	...	Y
1468	...	...	...	...	N
1496	...	×	...	×	Y
1656	...	...	...	...	N
1927	...	...	...	...	N
1991	...	...	...	...	N
2052	×	×	...	...	Y
2063	...	...	...	...	N
2151	...	...	...	...	N
2199	...	...	×	×	Y
2634	×	...	×	...	Y

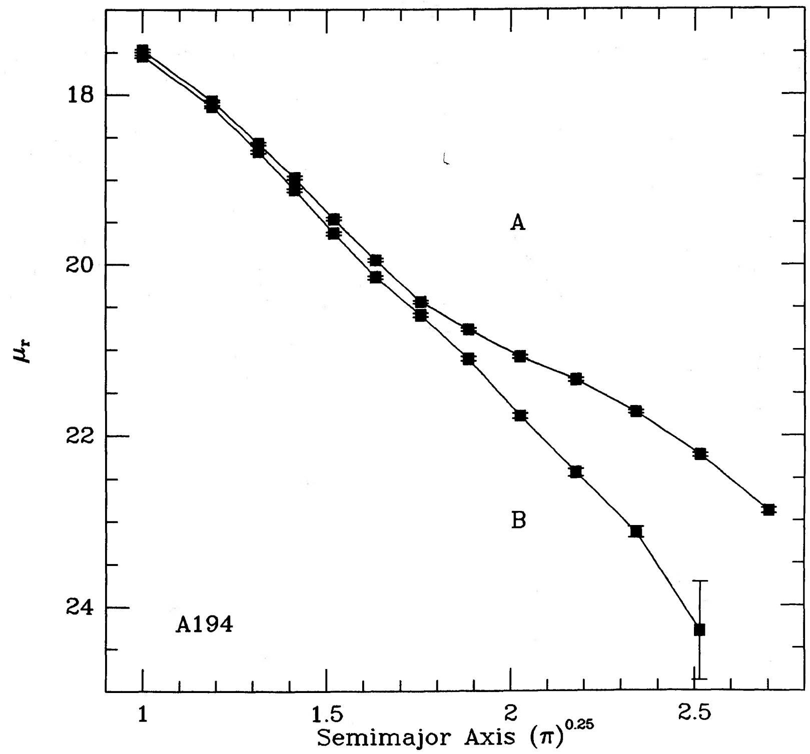

FIG. 20.—Surface photometry profiles for the components of A194 as a function of semimajor axis length in arcseconds to the quarter power. Central surface brightnesses of the components are not shown.

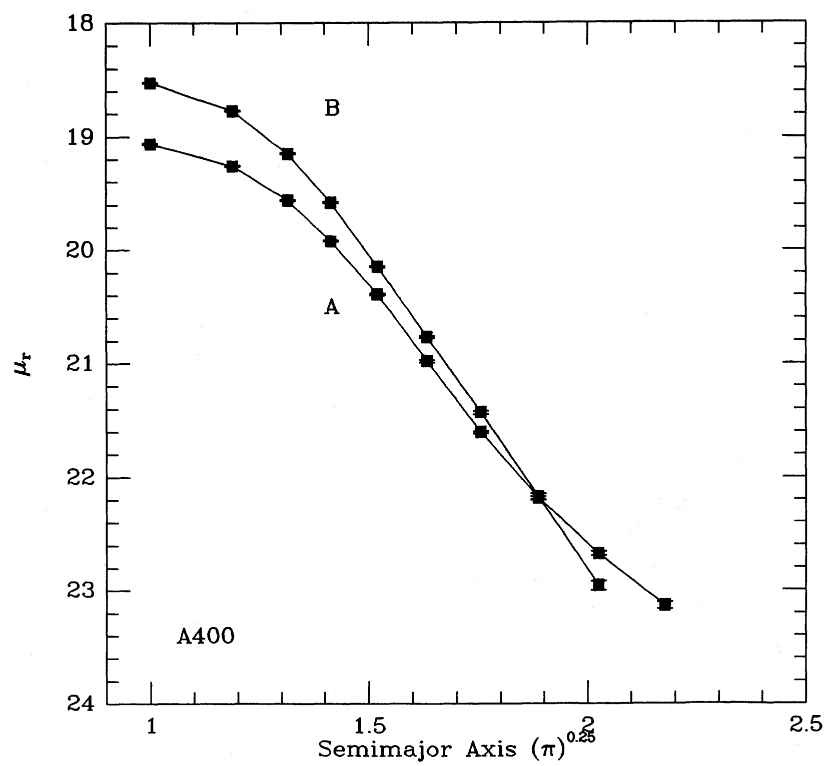

FIG. 21.—Surface photometry profiles for the components of A400 as in Fig. 20

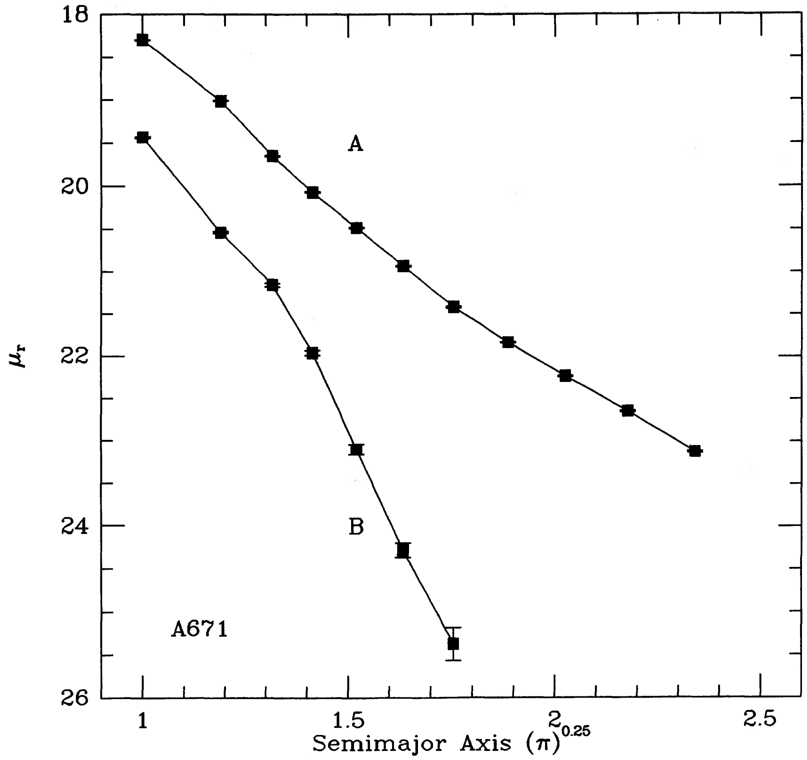

FIG. 22.—Surface photometry profiles for the components of A671 as in Fig. 20

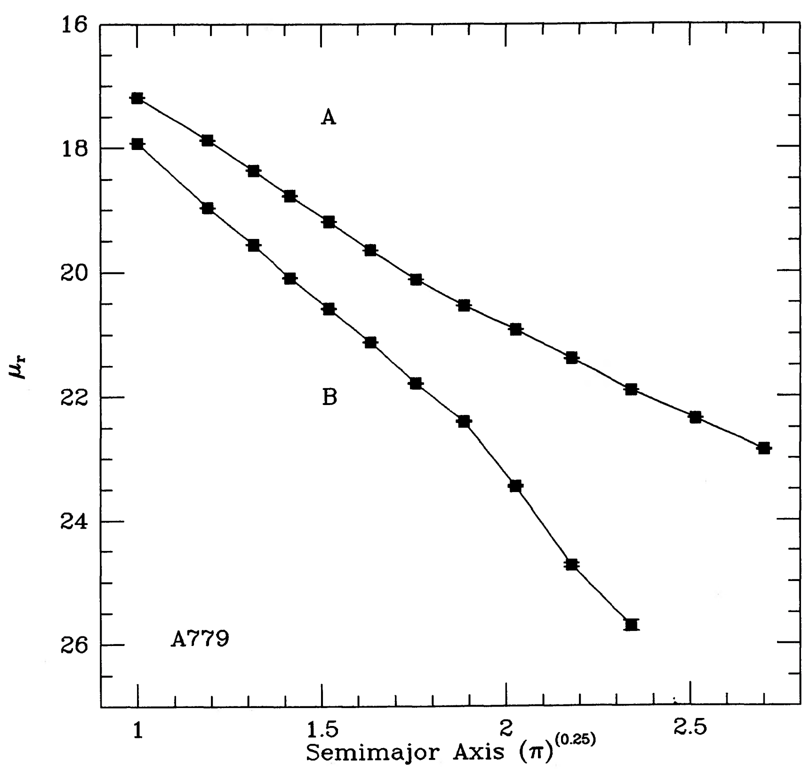

FIG. 23.—Surface photometry profiles for the components of A779 as in Fig. 20

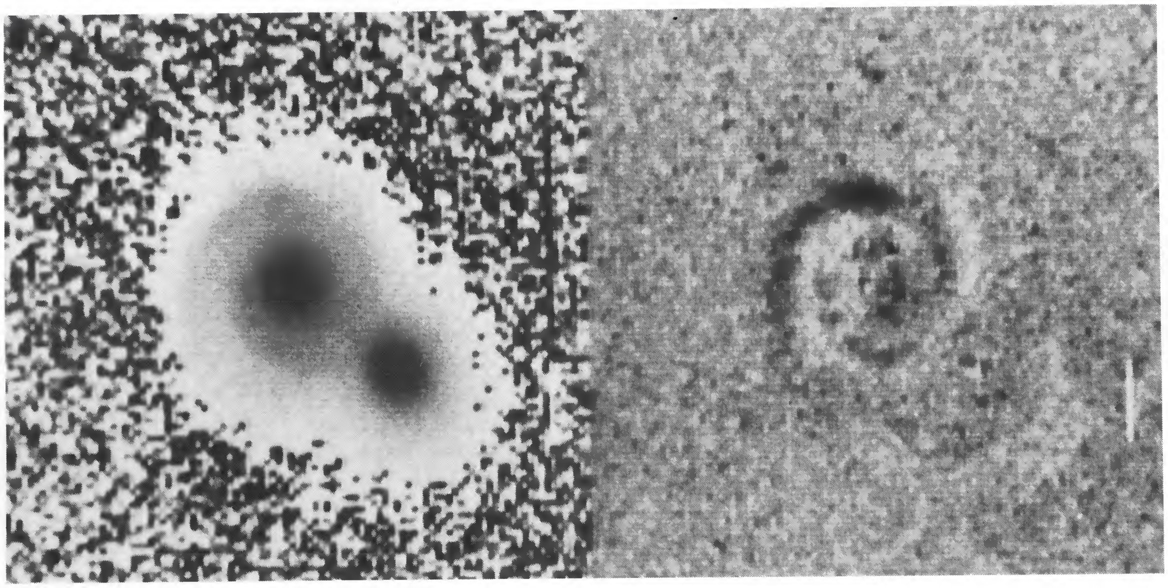

FIG. 9.—CCD image and residual map of the A1496 system as in Fig. 1. Each panel is 33″ on a side. Note the spiral-like patterns in the residual map around A1496A.

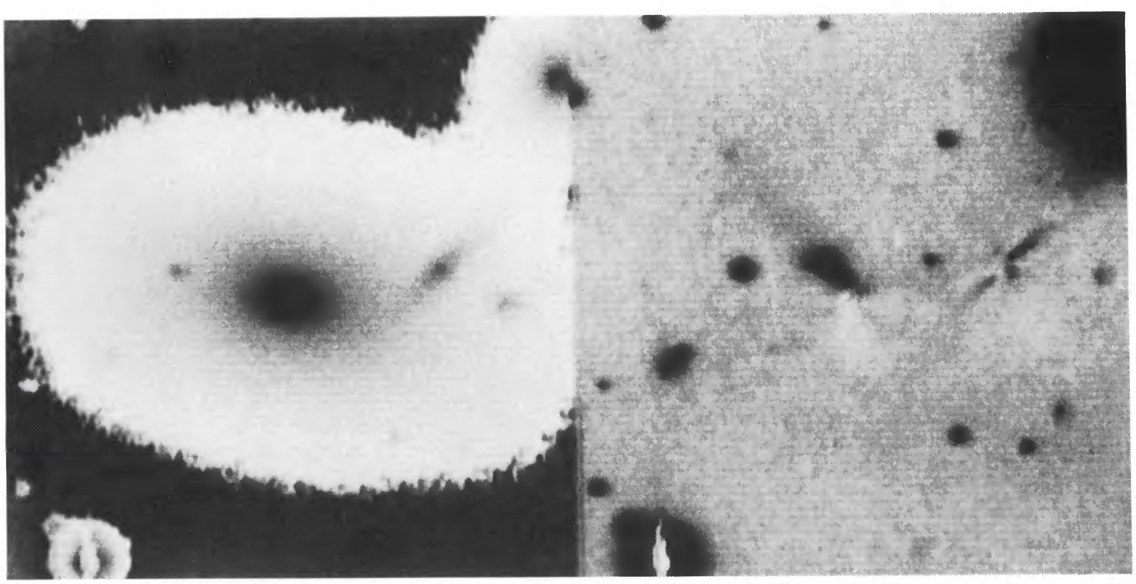

FIG. 10.—CCD image and residual map of the A1656 system as in Fig. 1. Each panel is 100″ on a side. The residual image is flat, but for reflections of A1656A's nucleus to the NW, and the disk of A1656B, which was not fitted.

LAUER (*see* **325**, 50)

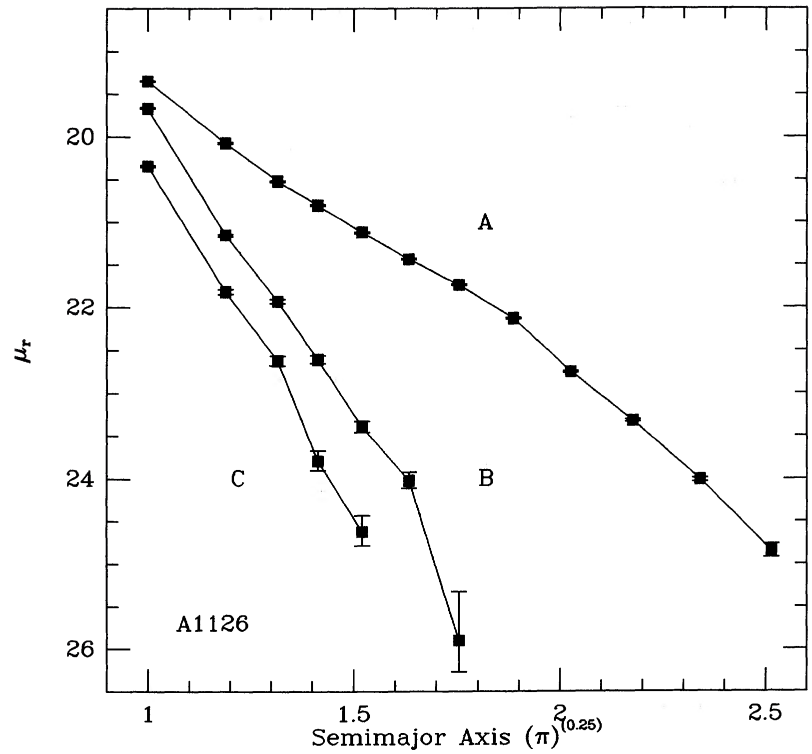

FIG. 24.—Surface photometry profiles for the components of A1126 as in Fig. 20

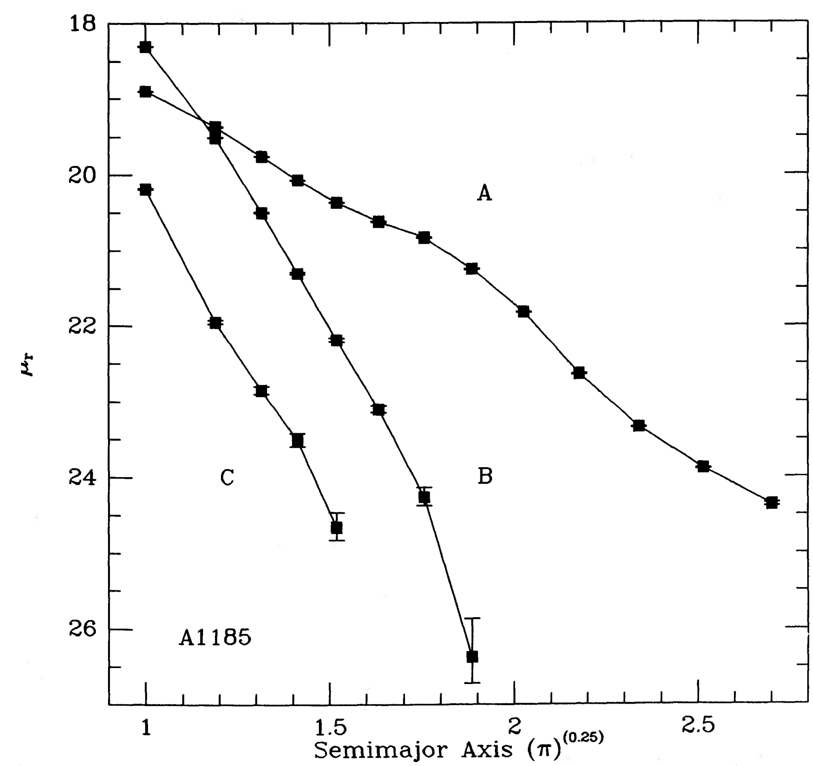

FIG. 25.—Surface photometry profiles for the components of A1185 as in Fig. 20

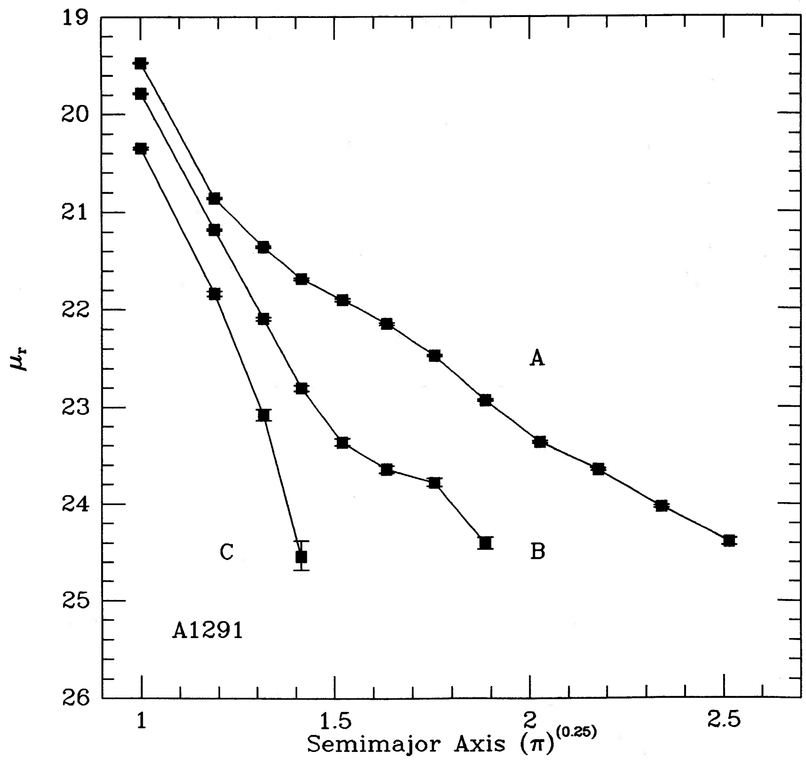

FIG. 26.—Surface photometry profiles for the components of A1291 as in Fig. 20

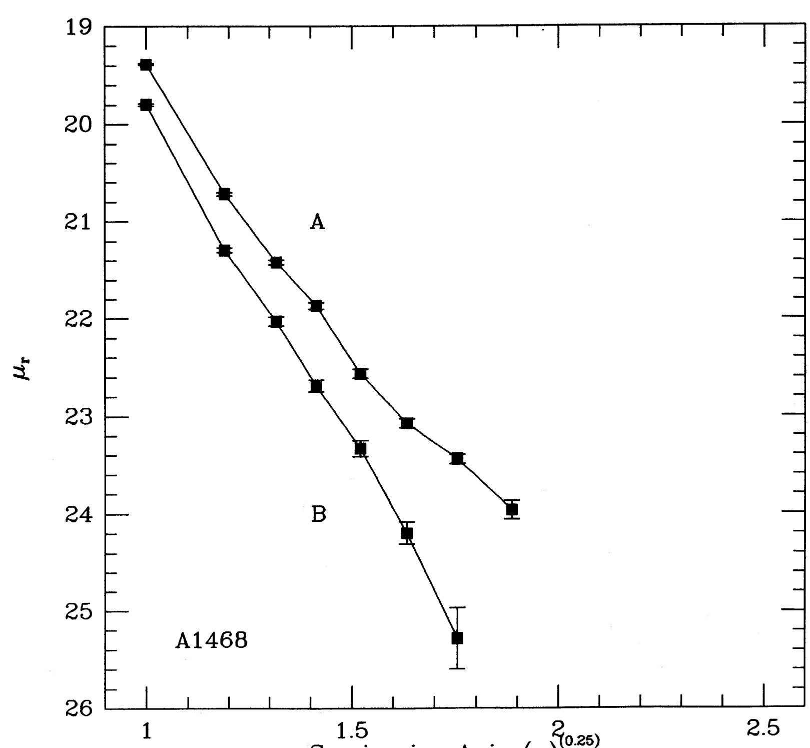

FIG. 27.—Surface photometry profiles for the components of A1468 as in Fig. 20

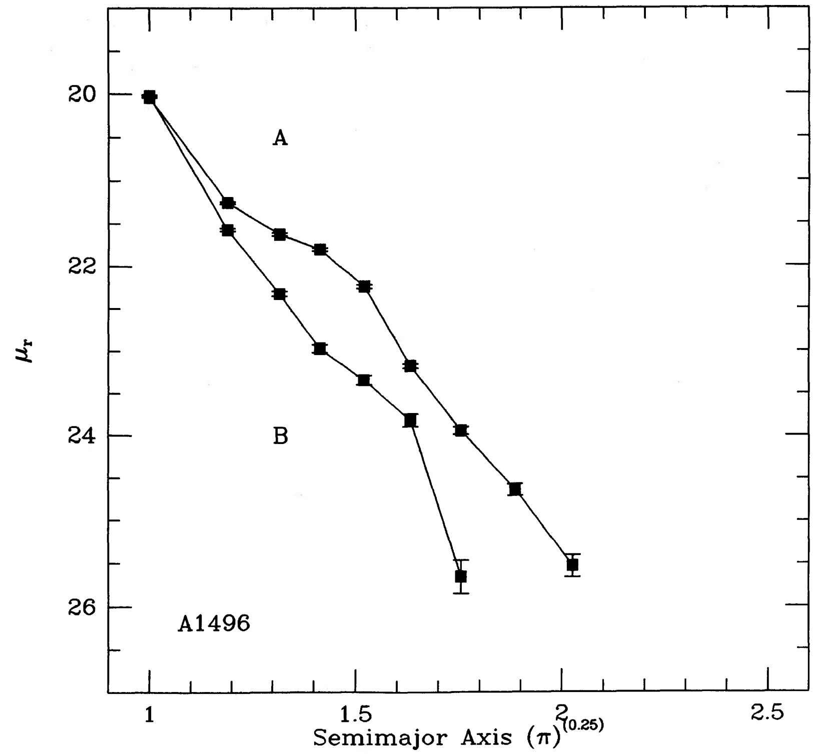

FIG. 28.—Surface photometry profiles for the components of A1496 as in Fig. 20

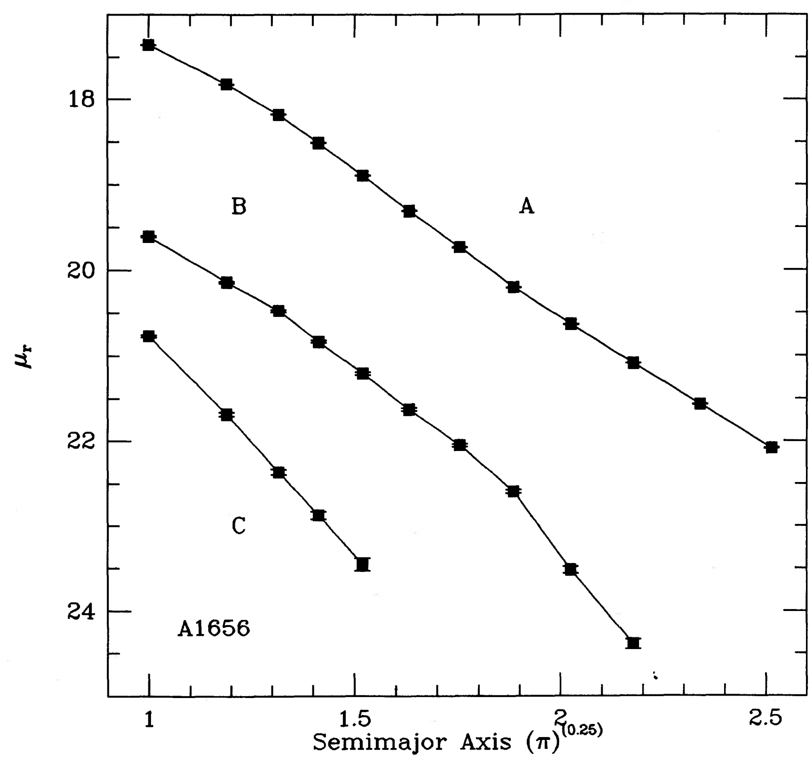

FIG. 29.—Surface photometry profiles for the components of A1656 as in Fig. 20

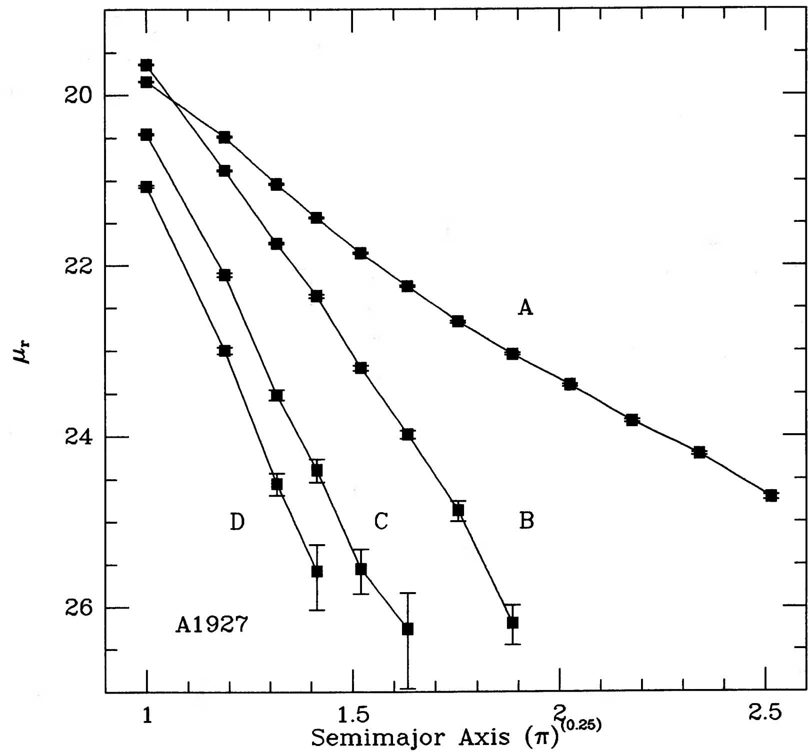

FIG. 30.—Surface photometry profiles for the components of A1927 as in Fig. 20

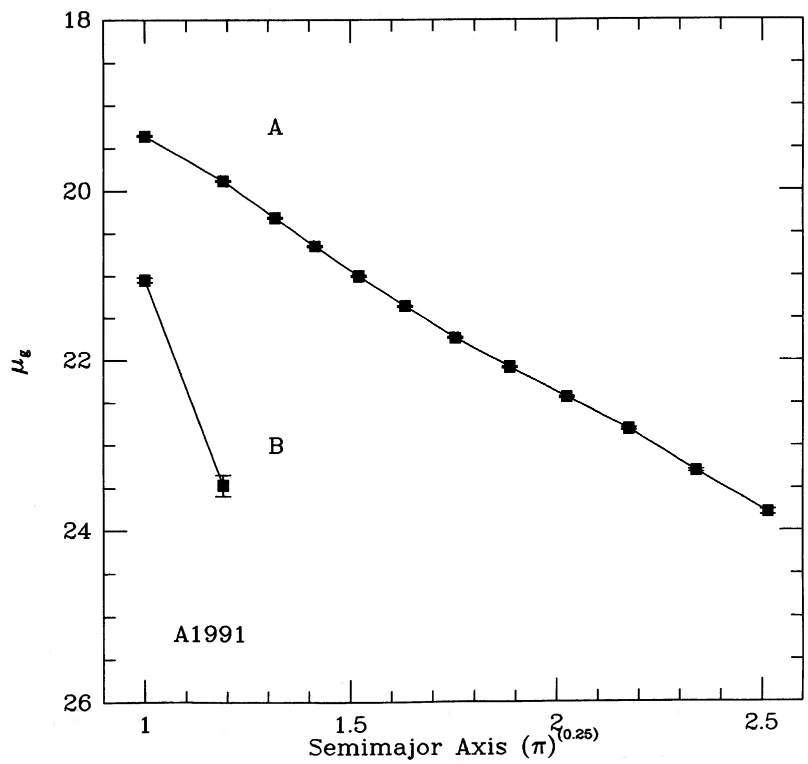

FIG. 31.—Surface photometry profiles for the components of A1991 as in Fig. 20

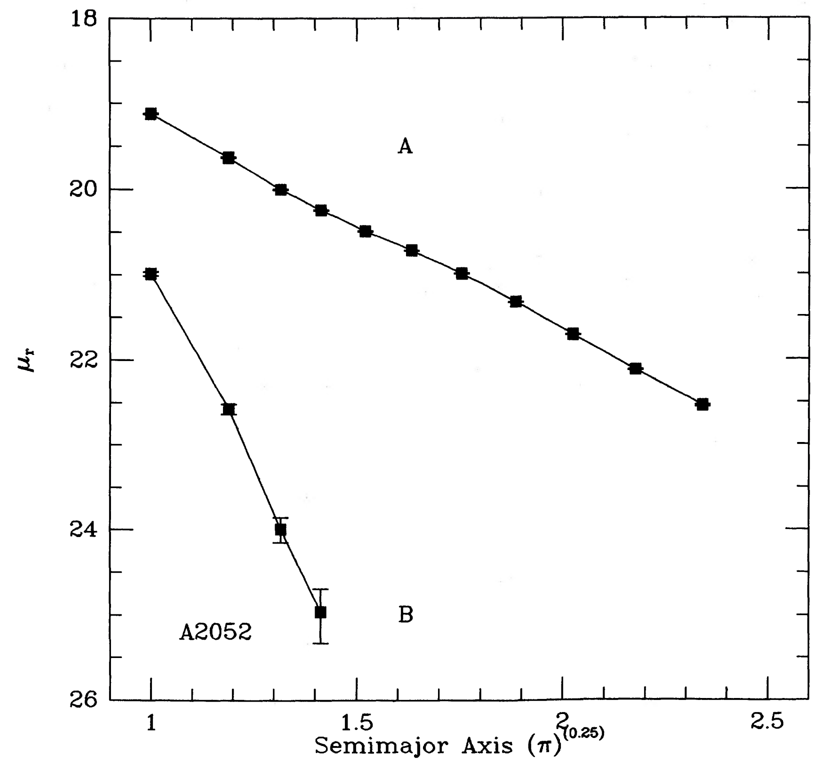

FIG. 32.—Surface photometry profiles for the components of A2052 as in Fig. 20

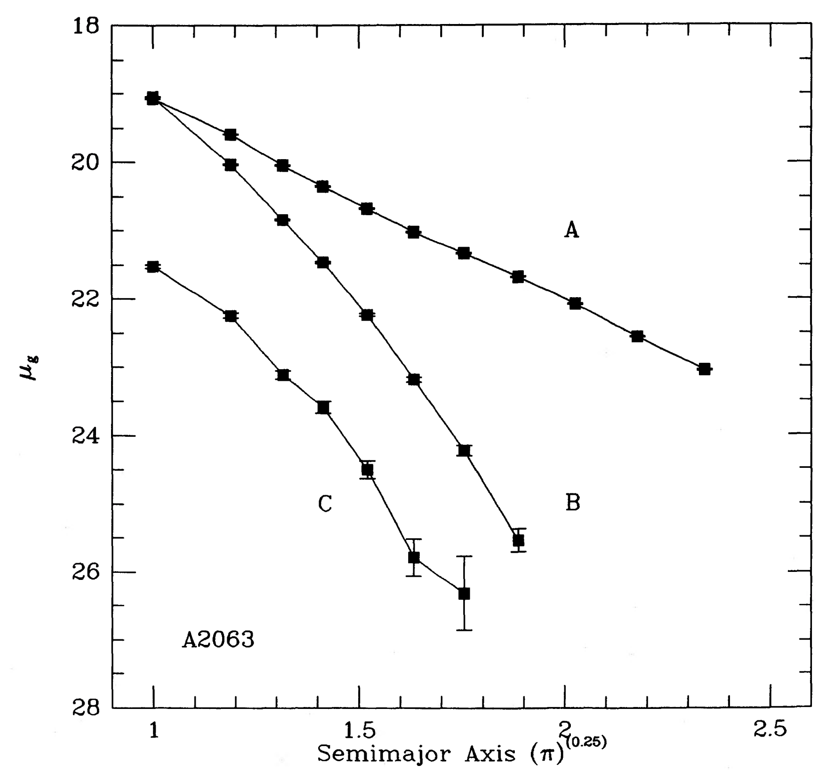

FIG. 33.—Surface photometry profiles for the components of A2063 as in Fig. 20

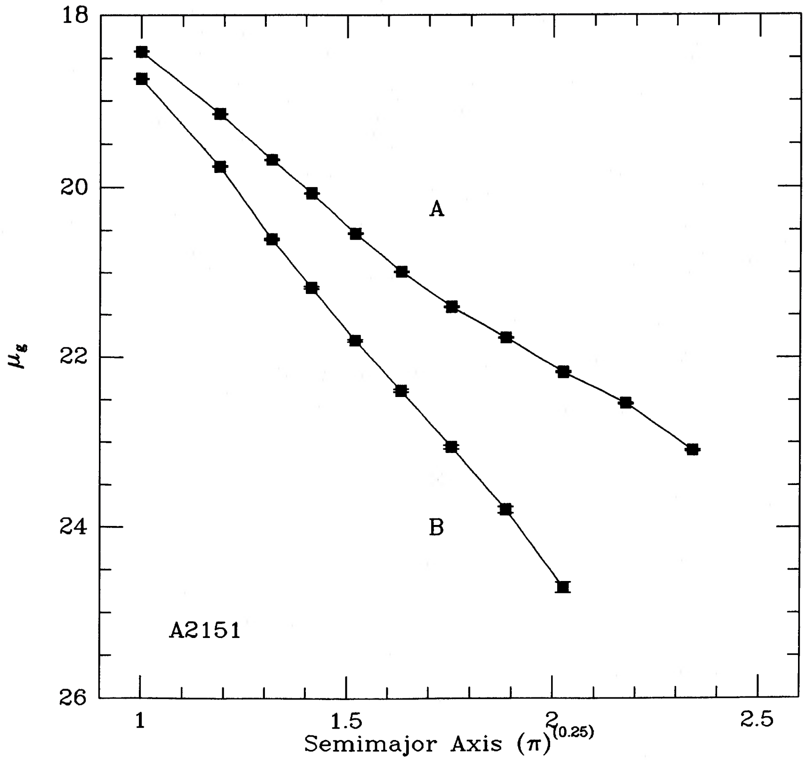

FIG. 34.—Surface photometry profiles for the components of A2151 as in Fig. 20

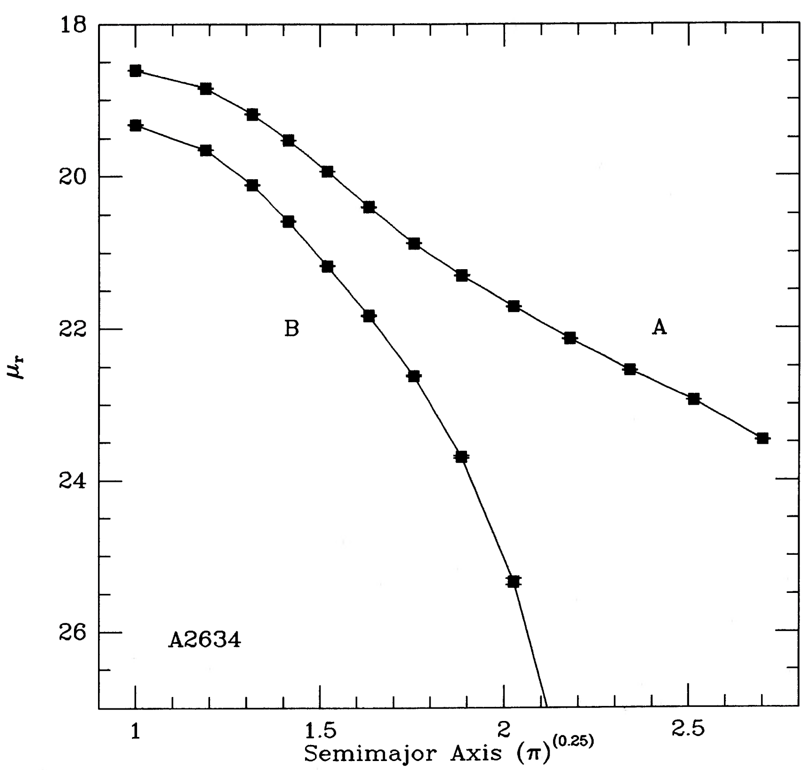

FIG. 35.—Surface photometry profiles for the components of A2634 as in Fig. 20

visible 10″ north of the nucleus. The picture presented is that the envelope center of mass of B at 3 kpc from its nucleus is displaced north of its nucleus by ~50 pc, while the envelope outside 6 kpc is shifted ~200 pc to the south. As discussed in § IV*a*, noncentric isophotes appear to be an excellent indicator of physical interaction between components in multiple systems; however, in this system such an interpretation can only be made tentatively. The distortions occur at a subtle level, and the present image was obtained under extremely poor seeing conditions; a separate image obtained by John Tonry under better seeing conditions, but with poorer signal-to-noise does not confirm these results. Independent of this problem, interaction between A and B may be supported by the VLA observations of Owen *et al.* (1985). Both galaxies emit similar double-sided jets that show similar bends and twists to the east, arguing that the galaxies are indeed physically close. The radial velocity difference between the galaxies is fairly large, 426 kms^{-1}, and is indistinguishable from the cluster dispersion of 423 km s^{-1}, arguing for an unbound encounter. On the other hand, the velocity difference between and A and B is still small enough, given their central dispersions (Tonry 1985*a*), to be consistent with a bound system if their velocity vectors are close to the line of sight.

iii) *A671*

The extra "nucleus" (B) in this system appears to be a low-luminosity galaxy with high ellipticity. There is no evidence for physical interaction between it and the central bright galaxy (A). Despite the high ellipticity of B, its isophotes are still well described as pure ellipses; the residual map shown in Figure 3 is smooth and shows no features inconsistent with simple superposition. A671A has a pure power-law profile, while that of A671B appears to be exponential. Neither galaxy shows any sign of isophote twisting.

iv) *A779*

The secondary galaxy in this system, A779B (NGC 2831), appears to be differentially truncated and warped by tidal interactions with A779A, the cD galaxy NGC 2832. This is intriguing since the relative radial velocity of the two galaxies is 1692 km s^{-1}; this system presents an excellent chance to observe the effects of high-speed in galaxies. The truncation of A779B is visible in its brightness profile (Fig. 23), which begins falling below a normal $r^{1/4}$ law outside of 13″ (~7 kpc). Further, an arc of negative residuals is visible between the two galaxies (see Fig. 4), consistent with even stronger truncation of galaxy B in the direction toward the cD nucleus; the implied differential truncation is over 1 mag in surface brightness for the envelope of B at radii greater than 10 kpc from its nucleus. The isophotes of A779B also show a strong twist, 60° from its core to the last isophote measured, toward alignment with the internucleus line (Fig. 36). Both the truncation and warping of A779B are visible in its contour map (Fig. 37). Galaxy A itself has a normal power-law brightness profile but shows a smooth 30° twist over the inner 10″ of its envelope, an unusual occurrence in a galaxy of high ellipticity. Lastly, an elongated faint diffuse feature is visible along the internucleus line that may be a dynamical friction wake induced in the envelope of A779A by the rapid passage of A779B. The feature is slightly contaminated by a reflection from the bright nucleus of B, but it is both more extended and brighter than the reflections from A779A (visible northwest of its nucleus), which itself has a more extended and brighter core than A779B.[1] The apparent magnitude of the feature corrected for the reflection from *B* is $m_B = 20.4$.

[1] The nuclei of both galaxies were overexposed and had to be filled in by properly scaled shorter exposures.

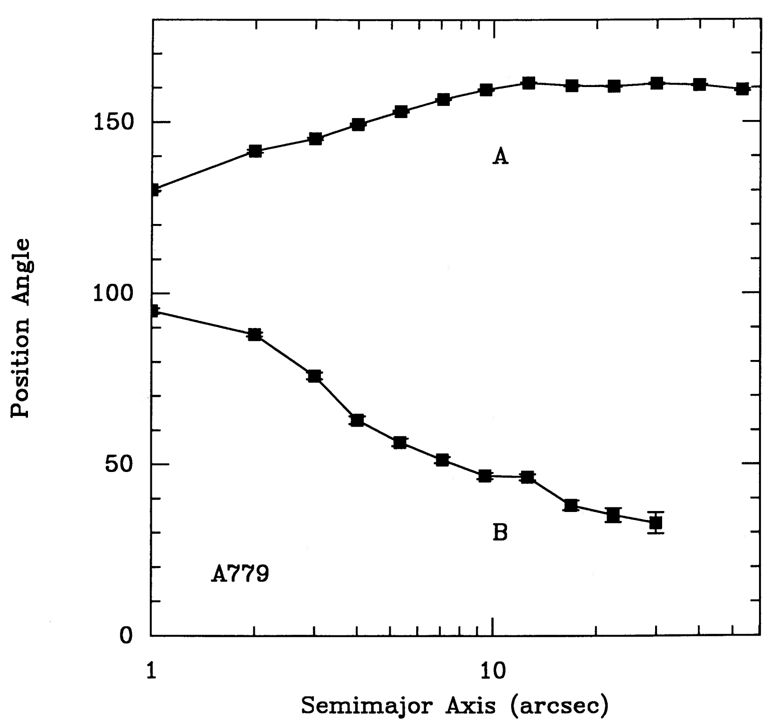

FIG. 36.—Isophote position angle profiles for the components of A779 as a function of semimajor axis length in arcseconds

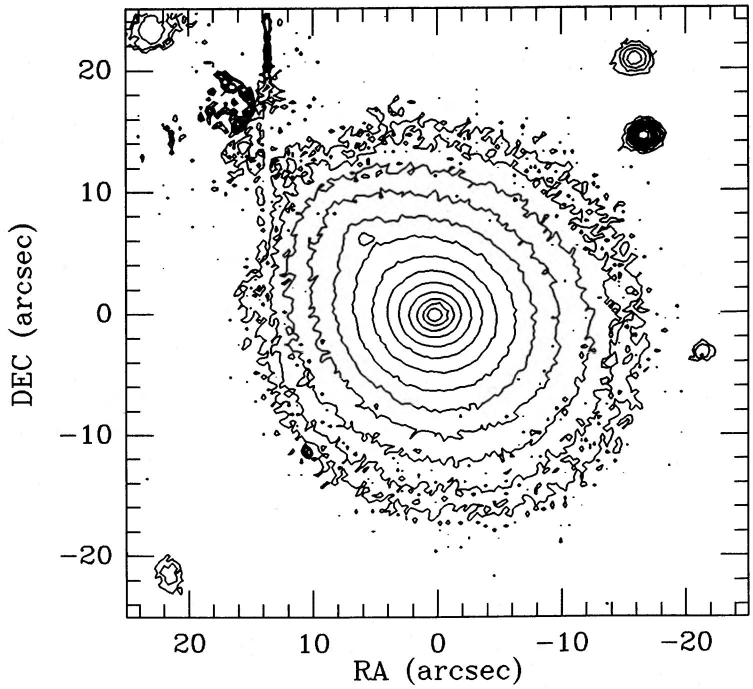

FIG. 37.—Contour map of A779B. Contours fall off in half-magnitude steps, beginning with the central contour of 18.0 mag arcsec^{-2} (r band).

v) *A1126*

Three galaxies were fitted in this system. There is weak but suggestive evidence for physical interaction. Diffuse patches of emission are visible in the residual map (Fig. 5) extending to the north from the nucleus of galaxy B and to the south of the nucleus of the central galaxy A that may be a dynamical friction wake. The contrast of the patches against the background galaxies is low, only 3% in surface brightness, but significant, given their extent. The relative velocity of A and B is high, 1299 km s^{-1}, as required to produce a narrow wake. Other evidence of interaction may be the unusual brightness profile of A1126A, which increases abruptly in slope beyond 10″ from its nucleus (Fig. 24). One interpretation, suggested by other interacting systems discussed below is that A1126A shows excess emission between 15 and 34 kpc from its nucleus over a simple $r^{1/4}$ law fitted to its entire envelope. Galaxies B and C themselves appear to be undisturbed, and their brightness profiles are consistent with $r^{1/4}$ laws.

vi) *A1185*

There is evidence for strong tidal interaction among the three galaxies comprising this system, a conclusion also reached by Hoessel, Borne, and Schneider (1985). The isophote centers of the central galaxy A1185A show large displacements from its nucleus that even change sign as a function of radius. The inner regions of A are first displaced from its nucleus toward C, the low-luminosity component to the southwest; isophotes of radius ~ 10 kpc have centers displaced by 1.4 kpc and are also distorted into an egg-shaped appearance (see Fig. 38). At larger radii still, however, the envelope of A is displaced in the *opposite* direction toward B instead of C; isophotes of radius ~ 30 kpc have centers offset 2.5 kpc to the northwest of the nucleus. The shift of the inner isophotes toward C is most easily seen as the strong dipole pattern of residuals visible in Figure 6. The opposite shift of the outer isophotes is also visible in the residual map by careful comparison of the northeast and southwest corners of the field and is easily seen directly in the stretched version of the original image in the left panel of Figure 6 and in the contour map of A1185A alone (Fig. 38). The brightness profile of galaxy A is also disturbed, showing excess light over a simple $r^{1/4}$ law from 5″ to 23″ (Fig. 25), even when the decomposition algorithm was allowed to follow the shifting centers of isophotes. The profiles of B and C appear to be normal $r^{1/4}$ laws, but this result should not be given too much weight, given difficulties with the decomposition done here. Galaxy B has a very low radial velocity difference with A, 57 km s^{-1}, while C has a difference of 534 km s^{-1}. The strong distortions of A1185A argue for a slow encounter and thus implicate galaxy B as their source. Galaxy C may also be in tidal contact with A1185A, however. As in A779, a faint diffuse feature ($m_B \approx 23$) is visible between the nuclei of galaxies A and C superposed on the background dipole residual pattern that may also be a dynamical friction wake.

vii) *A1291*

This also appears to be a system of interacting galaxies. The isophotes of the central galaxy beyond radii of 10 kpc are not centered on its nucleus and are pulled toward galaxy B, with the offset increasing steadily to 2.0 kpc at radii of ~ 20 kpc, as is visible in the left panel of Figure 7 and the contour map of A1291A alone (Fig. 39). Failure of the decomposition algorithm to handle nonconcentric isophotes is visible in the residual map, which shows an extended band of excess emission between A and B and a deficit of emission in the anti-B direction from A. As in the other apparently interacting systems, the brightness profile of A is also disturbed, showing excess emission over a simple $r^{1/4}$ law, which peaks at ~ 14 kpc from its nucleus (Fig. 26). The brightness profile of galaxy B appears distended at large radii. In contrast, galaxy C appears to be a normal low-luminosity elliptical, and shows no evidence of interaction with A or B.

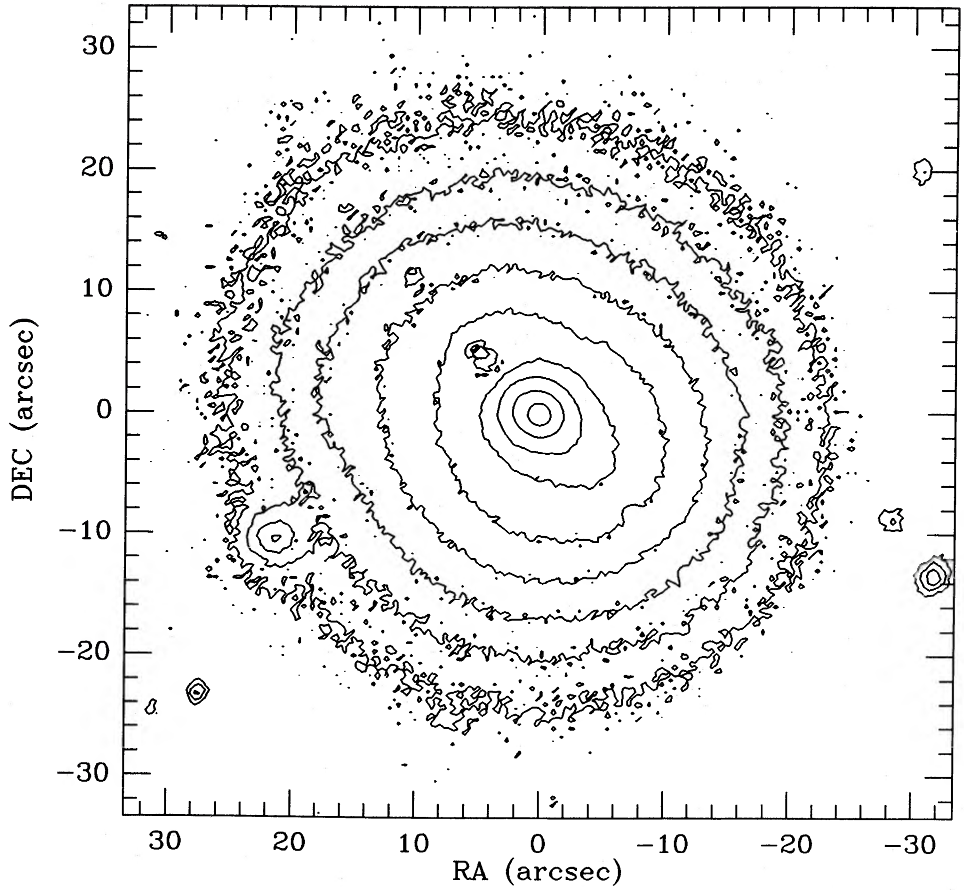

FIG. 38.—Contour map of A1185A. Contours fall off in half-magnitude steps, beginning with the central contour of 19.0 mag arcsec^{-2} (r band).

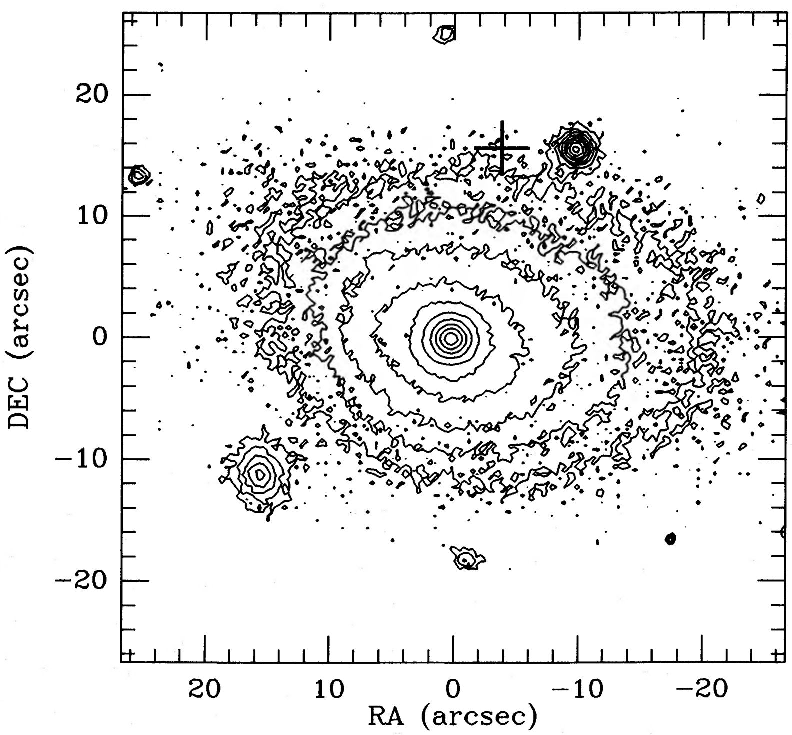

FIG. 39.—Contour map of A1291A. Contours fall off in half-magnitude steps, beginning with the central contour of 19.5 mag arcsec^{-2} (r band). Large cross marks the central location of A1291B.

viii) *A1468*

This is another binary system of galaxies with similar brightnesses. No evidence for interaction between the galaxies was found, consistent with the observations of Smith *et al.* (1985), who show that A1468B must be a background galaxy since its velocity difference with respect to A1468A is over 12,000 km s^{-1}. The residual map shown in Figure 8 is flat, showing no global isophote distortions of either galaxy or any faint tidal features. The brightness profile of A appears to be a normal power law, while galaxy B follows a normal $r^{1/4}$ law.

ix) *A1496*

This may be another system of interacting galaxies; however, its morphology is unique among the current sample. As can be seen in Figure 9, the central galaxy appears to have a faint spiral arm which wraps most of the way around its nucleus. Further, the inner brightness profile of A1496A shows a highly localized excess of emission over an $r^{1/4}$ law fitted to its outer isophotes (see Fig. 28), even after pixels contaminated by the spiral arm were excluded from the decomposition; the "excess" peaks at ~ 0.5 mag 10 kpc from the nucleus. Toomre (private communication) suggests that the central galaxy is an S0 disturbed by a strong encounter with A1496B.

x) *A1656*

The central galaxy is NGC 4889, the brightest elliptical in the Coma cluster. The secondary galaxies are RB77 (B), an apparent S0 galaxy, and RB75 (C), a low-luminosity elliptical galaxy. There is no evidence of interaction between these galaxies. As is seen in Figure 29, both NGC 4889 and RB75 follow normal $r^{1/4}$ laws, while the profile of RB77 is consistent with an undisturbed exponential disk. The sharp disk of RB77, of course, is poorly described by the elliptical isophotes used by the decomposition procedure, and is clearly visible in the residual map (Fig. 10). The disk shows no sign of warping, however, and no isophote twisting is seen in any of the three galaxies. A path of emission immediately to the northeast of the nucleus of NGC 4889 is apparent in the residual map, but this is almost certainly due to internal reflections of its overexposed nucleus in the camera optics.

xi) *A1927*

This is a complex system of several low-luminosity elliptical galaxies surrounding a central cD. The three most central galaxies were fitted along with the cD. Despite the complexity of this system, the decomposition algorithm worked extremely well. The residual map visible in Figure 11 is flat and shows no global patterns of residuals from distorted isophotes or tidal plumes. A1927A has a normal power-law profile, and the three secondary galaxies all have normal $r^{1/4}$ law profiles. There is no evidence that any of the four galaxies are interacting with each other.

xii) *A1991*

The secondary galaxy in this system is an extremely low-luminosity galaxy to the west of the central cD. There is no evidence that this galaxy is interacting with the cD at present or that the cD itself is disturbed in any way. The residual map in Figure 12 is flat, and the cD galaxy appears to follow a normal $r^{1/4}$ law. The nature of A1991B itself is poorly determined, given its limited angular extent and low luminosity. It does appear to be a galaxy, however, since its apparent core is larger than the seeing radius.

xiii) *A2052*

As in A1991, the secondary galaxy is a low-luminosity component apparently embedded in the envelope of a central cD galaxy; in this case, however, the galaxies appear to be interacting. The isophotes of the cD galaxy are not concentric, as the strong dipole pattern of residuals in Figure 13 shows. The nucleus centroid is displaced to the northwest by ~ 0.2 kpc from the center of isophotes 5.0 kpc out and by ~ 0.7 kpc from isophotes 12 kpc from the nucleus. Further, the inner portions of the cD brightness profile rise slightly above a normal $r^{1/4}$ law defined by the outer isophotes, with a maximum deviation of 0.15 mag at 11 kpc from the nucleus. Malumuth (private communication) finds that the velocity dispersion profile rises abruptly to a local maximum near this point.

xiv) *A2063*

Two secondary galaxies are seen against the central cD galaxy. There is no evidence for physical interaction between any of the three galaxies. The residual map is flat (Fig. 14) and A2063A and A2063C have $r^{1/4}$ law brightness profiles. A2063B has complex residuals around its core and may have a weak disk component. Its brightness profile appears to be exponential.

xv) *A2151*

The central galaxy in this system is NGC 6041, the brightest galaxy in the Hercules cluster. The secondary galaxy appears to be an S0; an edge-on disk is visible in both panels in Figure 15. NGC 6041 itself appears to have a central dust lane running parallel to its *minor* axis, visible in the residual map. The residual map is otherwise flat, however, and shows no distortion of either galaxy or any faint tidal features. The profile of NGC 6041 follows a normal power-law profile, and A2151B follows a normal $r^{1/4}$ law. There is no evidence for physical interaction between the two galaxies.

xvi) *A2634*

The central galaxy in this system, the cD galaxy NGC 7720, appears to be interacting with the secondary galaxy to its north. As can be seen in both panels in Figure 16 and the contour map in Figure 40, the cD nucleus is displaced from its envelope in the direction toward the secondary (this result is confirmed by separate images obtained at Lick Observatory). Isophotes around the cD appear to share a common center for radii within 13 kpc of its nucleus; however, isophotes with radii of 17 kpc have centers displaced from the nucleus by ~ 0.5 kpc, and the offset increases rapidly to 5.1 kpc for isophotes 47 kpc out from the nucleus. The relative velocity of the two galaxies is 997 km s^{-1}, which implies that, like A779, this is another example of a high-speed interpenetrating encounter. The secondary galaxy itself has a strongly truncated brightness profile, with isophotes that twist 30° in the direction toward the cD. The residual map in Figure 16 shows that this truncation appears to be more severe on the side of A2634B facing the nucleus of the cD. The residual map also shows a broad band of excess emission running along the major axis of A2634A south of its nucleus; this may be material stripped from A2634B.

IV. INTERACTION EFFECTS

a) *Noncentric Isophotes*

Nonconcentric isophotes around galaxies in multiple systems present the strongest evidence for components in tidal

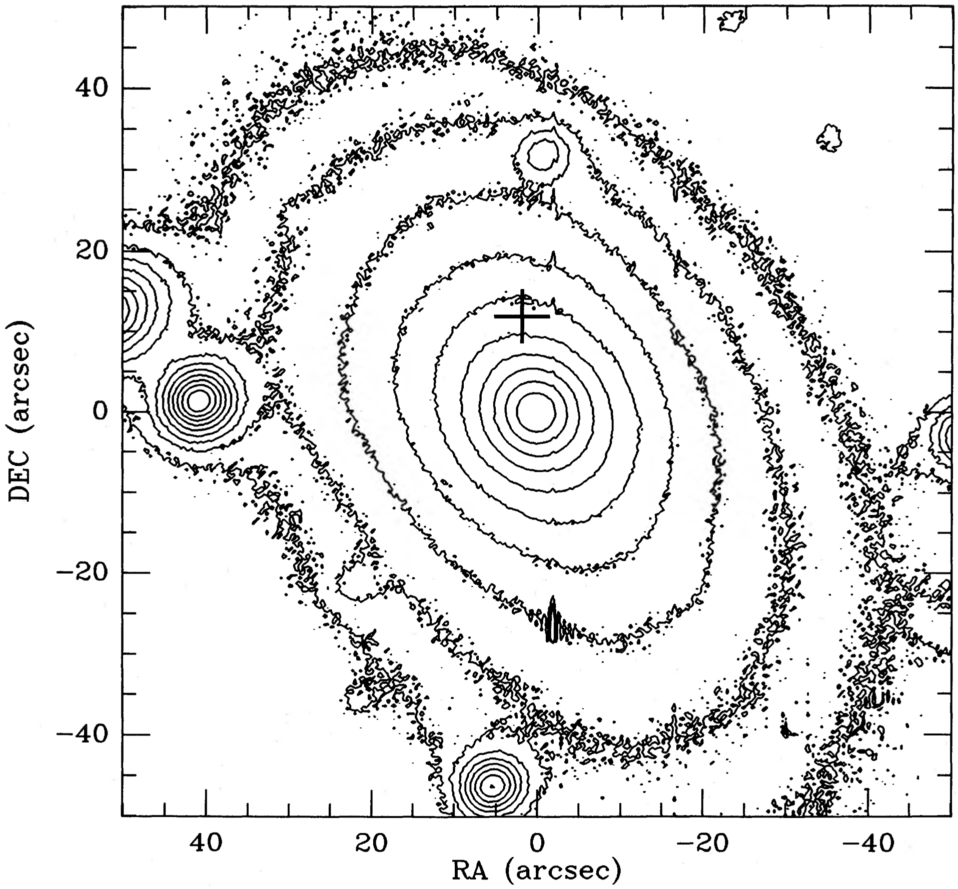

FIG. 40.—Contour map of A2634A. Contours fall off in half-magnitude steps, beginning with the central contour of 19.0 mag arcsec^{-2} (r band). Large cross marks the central location of A2634B.

contact. Both Borne (1984) and Aguilar and White (1986) using N-body simulations have shown that strong asymmetric envelope distortions can result from tidal interactions between galaxies. Further, while nonconcentric isophotes are common in the present sample, they are rarely seen in isolated elliptical galaxies; in a sample of 42 normal elliptical galaxies, Lauer (1985) found no evidence for nonconcentric isophotes. A convenient way to describe isophote offsets is by the ratio $\Delta R/R$, where R is the isophote radius and ΔR is the displacement of its center from the nucleus; an average upper limit for $\Delta R/R$ from the sample of Lauer (1985) is $\sim 0.5\%$ over the inner ~ 5 kpc of the galaxies. In contrast, the central galaxies in A1185, A1291, and A2634 all have envelopes displaced from their nuclei with $\Delta R/R > 10\%$ at some radii. A499 and A2052 have more modest maximum displacements of 3% and 6%, respectively, but these still create obvious patterns in their residual maps; galaxies assumed to have *concentric* isophotes in this study in general must have $\Delta R/R < 1\%$.

A displacement of a nucleus from its envelope will quickly decay away and thus must reflect recent tidal perturbations, implicating nearby galaxies as the perturbers. A simple way to look at this problem is to assume that the nucleus receives a velocity "kick" from an incoming perturbing galaxy, which is then opposed by dynamical friction with the surrounding envelope. The "nucleus" is defined here as the portion of the galaxy within a radius r from its center such that the crossing time $t_c \approx r/\sigma$ is less than the encounter time $T \approx a/V$, where σ is the velocity dispersion of the galaxy, and a and V are the impact parameter and encounter velocity of the perturber; the "edge" of the nucleus is set at radius d at which $t_c = T$. The nucleus thus will respond as a more or less solid body within an envelope responding to differential impulsive tidal effects. This appears to be a reasonable assumption; $\Delta R/R$ decreases inward for all galaxies with nonconcentric isophotes and goes to zero at limiting inner radii for A1291A, A2634A, and A779B. Lauer (1986) calculates the growth of impulsive asymmetrical tidal distortions in an isothermal galaxy; relative to the envelope at radii near the impact parameter, the velocity impulse received by the nucleus is

$$\Delta v \approx \frac{\sigma^2 \sigma_i^2}{V^3}, \tag{1}$$

where σ_i is the velocity dispersion in the infalling perturber. This implies that for typical encounter velocities in rich clusters, $\Delta v \ll \sigma$; this conclusion appears consistent with the values of $\Delta R/R$ seen in the present sample which are always small in absolute size.

Dynamical friction sets the time scale for orbital decay of the nucleus back to the center of the surrounding envelope. The deceleration of the nucleus is given by

$$\frac{d\Delta v}{dt} = -4\pi G^2 m\rho f(x) \ln \Lambda \, \Delta v^{-2}, \tag{2}$$

see Chandrasekhar (1942), where m is the mass of the nucleus, ρ is the mass density of the surrounding envelope, $x = \Delta v/2^{1/2}\sigma$, and $f(x)$ gives the efficiency of the envelope for exerting a drag force. In general, $f(x) = \text{erf}\,(x) - x\,\text{erf}'\,(x)$; however, for $x \ll 1$, to second order $f(x) \approx 4/[(\pi)^{1/2}]x^3$. In this regime, the dynamical friction deceleration is directly proportional to the velocity of the nucleus. The characteristic decay time of the nucleus, $\tau \equiv -\Delta v/(d\Delta v/dt)$ is thus velocity independent; in other words, the particular value of Δv given by the simple approximations used to derive equation (1) is irrelevant provided it remains much smaller than σ. For an isothermal galaxy, $m = 2d\sigma^2/G$, and the envelope density outside the nucleus is $\rho = \sigma^2/(2\pi G d^2)$. This gives, taking $\ln \Lambda = 2$,

$$\tau = \frac{3\sqrt{2\pi}\,d}{16\sigma}\,. \tag{3}$$

In terms of the encounter time T, which is also the crossing time in the nucleus at d, $\tau/T \approx 0.5$; as stated above, nonconcentric isophotes are strongly damped and the perturbers will still be nearby.

It is noteworthy that the components in multiple systems with nonconcentric isophotes are usually the primary central galaxies. The secondaries are compact; as seen in Table 2, their median effective radius is less than 2 kpc. Such compactness works against the growth of asymmetric tidal distortions. The secondaries have a limited extent over which to "feel" the tidal field of their primaries, and their short nuclear crossing times will act to smooth over impulsive tides and to erase any asymmetries which would be created.

b) Brightness Profile Effects

i) *Tidal Limiting of Secondary Galaxies*

Secondary galaxies A779B, A2199B, and A2634B have brightness profiles that steepen at large radii, suggesting tidal truncation by their primaries; it may be that a number of other secondaries with exponential profiles may really be truncated $r^{1/4}$ laws, too. Simple calculations using the impulse approximation (Lauer 1986) show that even after a fast encounter, the outer envelope of a secondary galaxy may be stripped off outside a tidal radius, R_T, which is given by

$$R_T \approx \frac{a}{4}\left(\frac{\sigma_i V}{\sigma^2}\right). \tag{4}$$

For typical values of the parameters in equation (4), say $V \sim 1000$ km s^{-1}, $\sigma \approx 300$ km s^{-1}, and $\sigma_i \approx 200$ km s^{-1}, this gives $R_T \approx 0.5a$. Since the present photometry of the secondaries extends well over the projected separations from their primaries. For example, both A779B and A2634B have $R_T \approx$ recently passed within a few metric radii, $\sim$40 kpc, of their primaries. For example, both A779B and A2634B have $R_T \approx$ 16 kpc, suggesting encounters within $\sim$25 and $\sim$30 kpc, respectively, given the dynamics observations of Tonry (1985*a*); A2199B is discussed in Lauer (1986) and appears to have come within $\sim$20 kpc of A2199A. Milder first-order tidal effects, which will produce symmetric isophote twisting or stretching of the secondaries, may also occur. At one encounter time, T, after closest approach, symmetrical tidal distortions will have grown to

$$\frac{\Delta R}{R} \approx 4\sqrt{2}\left(\frac{\sigma}{V}\right)^2. \tag{5}$$

Again, for typical values of V and σ, symmetrical distortions should be readily apparent even as the encounters are in progress, a conclusion that is supported by the N-body simulations of Miller (1986).

Most secondary galaxies have profiles consistent with $r^{1/4}$ laws—the problem is to understand how this constrains any past interactions with their primaries. Aguilar and White (1986) have studied the effects of tidal interactions on the brightness profiles of galaxies in high-speed encounters. The work done by these investigators is not relevant to strong interactions of galaxies with large differences in mass, but may be of use in understanding the effects of more distant encounters than the ones considered above. In their N-body experiments Aguilar and White (1986) show that tidal mass loss in all but the weakest collisions produces remnants more compact than the original galaxies, but that still follow $r^{1/4}$ laws. In this context, it is interesting to look at the mass-radius relationship for all components in the present sample (Fig. 41). Figure 41 also plots the mass-radius relationship for the 42 galaxies studied by Lauer (1985) and that measured for galaxies within the central 1 Mpc of A2199 (Strom and Strom 1978*a*). As can be seen, the secondary galaxies (all of which have $M_B > -21.7$) are much more compact than normal elliptical galaxies, but fall close to the mean mass-radius relationship for the central population of A2199. Strom and Strom (1978*a*, *b*, *c*) in general find centrally located galaxies in rich clusters to be more compact than those in the cluster outskirts. In A2199, for example, these investigators show that the average effective radius of galaxies within its central 1 Mpc is half that of galaxies of the same luminosity outside the center. The mass-radius relationship for the present set of secondary galaxies thus appears to be that of a normal population of ellipticals within the center of a rich cluster; there does not appear to be

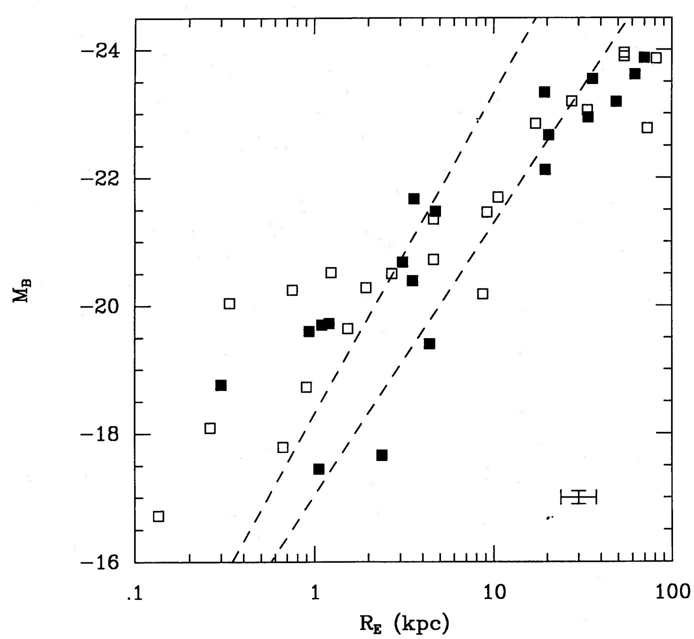

FIG. 41.—Magnitude-radius relationship for all components in the present sample (Table 2) and Lauer (1986). Solid symbols are for galaxies in noninteracting systems; open symbols are for galaxies in interacting systems (see Table 3). Dashed lines are magnitude-radius relationships measured by Strom and Strom (1978*a*) for the inner 1 Mpc of A2199 (*leftmost line*) and for galaxies in the outer regions of A2199 (*rightmost line*). Typical error bars for the magnitudes and radii of the less luminous secondary galaxies are shown in the lower right corner.

any evidence for more severe tidal ablation of the secondaries on average than that suffered by any galaxy near the cluster cores. On average there is also little evidence that secondaries associated with interacting systems are any more compact than those in noninteracting systems, although it may be significant that the most compact secondaries in interacting systems, A2052B, A1291B, A1185B, and A2634B are associated with the primaries showing the most nonconcentric isophotes. On the other hand, A1927D, which is in an apparently noninteracting system, is just as compact as these last four galaxies. A larger sample will be needed to see if the second galaxies in interacting systems are preferentially more compact; at the present, it is not possible to show that a secondary galaxy is *currently* interacting with the central galaxy based on its compactness alone.

ii) *Excess Light around Primary Galaxies*

Five central galaxies among the interacting systems (see Table 3) appear to have excess emission at intermediate radii (~ 10 kpc) over $r^{1/4}$ laws fitted to the entire extent of their brightness profiles; a simple interpretation of this result is that the primary galaxies have been puffed-up interior to some radius, giving their inner envelopes a shallower luminosity gradient relative to their outer envelopes. This "puffing up" appears to be elliptically symmetric around the primaries and thus is not due to material recently stripped off the secondary galaxies. Further, the unusual brightness profiles do not appear to be artifacts caused by failure of the decomposition algorithm to deal with interacting systems; A1126A has concentric isophotes, and the profile anomalies in A1185A and A2052A persist even when the decomposition algorithm follows their nonconcentric isophotes.

The dynamics of this present subset of interacting systems support the possibility that the central regions of their primaries may have been puffed up by tidal energy input from nearby secondary galaxies. All five systems have some secondary galaxies with relatively small radial velocity offsets, that is 321 km s^{-1} or less. In contrast, the remaining interacting systems, which have primaries with normal brightness profiles, only have secondaries with radial velocity differences in excess of 400 km s^{-1}. Tidal transfer of the secondaries' orbital energy into heating the primaries' envelopes is much stronger in low-velocity encounters; from equation (2) integrated over the encounter time shows that tidal heating of the primary goes as V^{-3}. This situation suggests the classical picture of galactic cannibalism presented by Hausman and Ostriker (1978), in which a central galaxy within a cluster puffs up as it drags in other galaxies within the cluster and converts their orbital energy into internal heat. While the structure of the central galaxy probably does not change homologously as these investigators assume, simple conservation of energy demands that the bulk of the central galaxy absorbing the orbital energy of the secondary must expand. If this picture is correct, then the observed profiles of the primaries are again transitory; the inner envelope will be too "hot" for its binding energy, and stars will move outward as the primary adjusts to a new equilibrium over a few dynamical times.

c) *Dynamical Friction Wakes*

Dynamical friction deceleration of a secondary galaxy passing through the extended envelope of a more massive galaxy creates a volume of enhanced background density, or "dynamical friction wake," that trails the secondary in its orbit; the faint diffuse feature visible near A779B, A1126, and A1185C, and between A2199B and A2199C, are suggestive of wakes. Weinberg (1986) has calculated wakes produced by point masses moving through an infinite homogeneous medium and by a satellite with an extended mass distribution orbiting an isothermal sphere. In both cases, the typical scale length of the wakes is of $R_S \equiv Gm/\sigma^2$, where m is the mass of the secondary and σ is the envelope velocity dispersion of the primary. Over the innermost scale length, the overdensity is of order unity, which, as argued below, may be enough to produce observable features. The quantity R_S is calculated and is given in Table 4, assuming $M/L_B = 5$, envelope dispersions given by Tonry (1985*a*),[2] and M_B from Table 2. The quantity R_S is typically a few kiloparsecs, similar to the observed extent of the wakes, R_W, also given in Table 4. Likewise, the morphology of the wakes calculated by Weinberg (1986) strongly resembles that of the features seen here. Wakes are dynamically hot and are thus smooth in appearance. The overdensity in the wakes falls off slowly (as r^{-1} in the infinite medium case), which produces diffuse and weakly condensed features, as observed, when the overdensity is integrated along the line of sight. Lastly, the cores of the wakes lag behind the secondaries as expected for wakes produced by extended galaxies.

The wake candidates are faint—Table 4 shows that the typical wake luminosity, L_W, is only $\sim 10^{-2}$ that of the associated secondary galaxy. The particular value of L_W contains information on the present position of the secondaries within their primary envelopes. Dynamical friction results from the gravitational attraction between the mass in the wake, m_W, and the secondary; m_W can be estimated crudely by treating it as a point mass and equating its direct gravitational effect on the secondary to the deceleration given by equation (2). This gives

$$\frac{Gm_W}{R^2} \approx 8\pi G^2 m\rho V^{-2} , \tag{6}$$

assuming $\ln \Lambda \approx 2$ and $f(x) \approx 1$, and where R is the distance between the wake and secondary. The results of Mulder (1983) and Weinberg (1986) show that the wake centers lag beyind the secondaries as $R \approx GmV/\sigma^3$; with equation (6) this gives

$$\frac{m_W}{m} \approx 0.028 \left(\frac{m}{10^{11}\ M_\odot}\right)^2 \left(\frac{300\ \text{km s}^{-1}}{\sigma}\right)^6 \left(\frac{\rho}{10^{-3}\ M_\odot\ \text{pc}^{-3}}\right) . \tag{7}$$

Masses of wakes calculated by this equation are similar to those estimated from Weinberg (1986). From equation (7) and L_W it is possible to estimate the local value of ρ surrounding

[2] No dispersion data were available for A1126. The envelope dispersion of A1126A is assumed to be 300 km s^{-1}.

TABLE 4

DYNAMICAL FRICTION WAKE CANDIDATES

Galaxy	L_W/L	R_S (kpc)	R_W (kpc)	ρ ($M_\odot$ pc^{-3})	d (kpc)
A779B	8.0×10^{-3}	4.8	5.3	6×10^{-4}	45
A1126B	2.3×10^{-2}	6.2	12	1×10^{-2}	58
A1185C	2.3×10^{-2}	1.2	5.0	1×10^{-2}	18
A2199B	5.4×10^{-3}	5.7	2.2	3×10^{-4}	87
A2199C	2.7×10^{-2}	1.1	2.2	4×10^{-2}	12

the secondary, which in turn leads to an estimate for the distance d of the secondaries from their primary nuclei.

Estimates of d are given in Table 4 for the galaxies with suspected wakes, from Abel inversion of the primary brightness profiles and assuming envelope $M/L_B = 10$. In all cases, $d > R_{sep}$, implying plausible locations of the secondaries; three galaxies, A779B, A1126B, and A2199B, have $d \gg R_{sep}$, giving ample room for errors in the simple calculations of m_W done here. The best case for a wake is the feature seen in A2199.[3] In addition to its diffuse appearance, it is also elongated with its major axis pointing to the nuclei of both A2199B and A2199C, consistent with the high velocities of both galaxies relative to A2199A. Further, the truncated profile of A2199B suggests that it has passed deep within the envelope of A2199A, within 20 kpc of its center, and is thus may still be within its envelope now. On the other hand, A2199C is less likely to be the source of the wake; it is much less massive than A2199B and must be much deeper within A2199A to produce a wake of the same strength, but its brightness profile is untruncated, showing no evidence for a strong encounter with A2199A.[4] The feature seen in A779 may also be a good wake candidate. The twisting isophotes of A779B and its asymmetrical truncation argue that it is in close contact with the central cD in A779 *now*; the strength of the truncation suggests that it has passed at least within ~ 25 kpc of the nucleus of A779A.

Note that the present results may lead to direct calculation of the orbits of A2199B and A779B. The estimated current distances of these two galaxies given in Table 4 from their primaries compared to their pericenter separations estimated above would imply that both galaxies are on highly eccentric orbits nearly parallel to the line of sight. Since the radial velocities of the galaxies thus must be nearly equal to their orbital velocities, this leads to an estimate of their apocenter distances. In an isothermal cluster, the apocenter distance, r_{max}, of a purely radial orbit is given by $r_{max} = r \exp [0.25(V/\sigma_{CL})^2]$, where r and V are the galaxy's current distance and velocity. For A779B, the parameters given in Tables 1, 2, and 4 give $r_{max} \approx 160$ kpc, and for A2199B, $r_{max} \approx 170$ kpc. The semimajor axes of both galaxies' orbits are thus ~ 90 kpc; calculations done in § V, and by Tonry (1985*b*), who models the orbital decay of galaxies of varying orbit eccentricities and sizes in a rich cluster with a massive central galaxy, show that both A779B and A2199B should survive cannibalism for several billion more years.

Similar calculations might be carried out for A1126A; however, A1126 is at a much higher redshift than A779 and A2199—its dynamical properties are poorly known and the wake barely detectable. A1126B may be truncated at large radii, permitting a pericenter estimate, but the errors in its last and only deviant isophote are large. Lastly, the faint feature in A1185 appears less likely to be a wake produced by A1185C and is more likely associated with the strong tidal distortions of the central galaxy. Again, as with A2199C, A1185B is a low-mass galaxy and can only produce a detectable wake if it is deep within its primary at a distance similar to its projected separation; considering the high velocities of both galaxies, this would imply that they are being observed at a very special time. In general, wakes are most likely to be visible with secondaries with luminosities $\gtrsim 1L^*$ in orbit around a primary with a large envelope, such as a cD galaxy. In the remainder of the present sample, A2634B is an obvious candidate for closer examination. A2634B is truncated, bright, and apparently interacting with the A2634, a cD galaxy; unfortunately its image was obtained in extremely poor seeing, which could easily render any wake undetectable.

[3] The existence of this feature has been confirmed by Kormendy (private communication).

[4] This conclusion supersedes the suggestion presented by Lauer (1986) that A2199C was the source of the wake, which was based on a preliminary analysis.

V. DISCUSSION

The results presented in Table 3 show that nine of the 17 systems studied here and in Lauer (1986) show morphological evidence for interaction between the primary and secondary components; if this sample is typical, then it may be concluded that $\sim 50\%$ of the multiple systems identified by Hoessel (1980), are composed of galaxies in physical contact. As discussed already, however, radial velocity observations make it clear that all interacting systems cannot be cases of cannibalistic merging. Systems in which solely high-velocity interactions ($\Delta V > 400$ km s^{-1}) between the secondaries and primaries take place are as common (four cases: A400, A779, A2199, and A2634) as systems in which *possible* low-velocity encounters are seen (only the radial velocities of the components are known, of course) that may be examples of classic cannibalism (the five systems identified in § IV*b*). In fact, it appears uncertain whether radial velocity observations alone can offer any *a priori* selection of interacting systems. Figure 42 shows the velocity distribution of the 19 secondaries within the metric radius measured by Tonry (1985*a*) and Smith *et al.* (1985) that could be normalized by the cluster velocity dispersions of Strubble and Rood (1986). The distribution can be

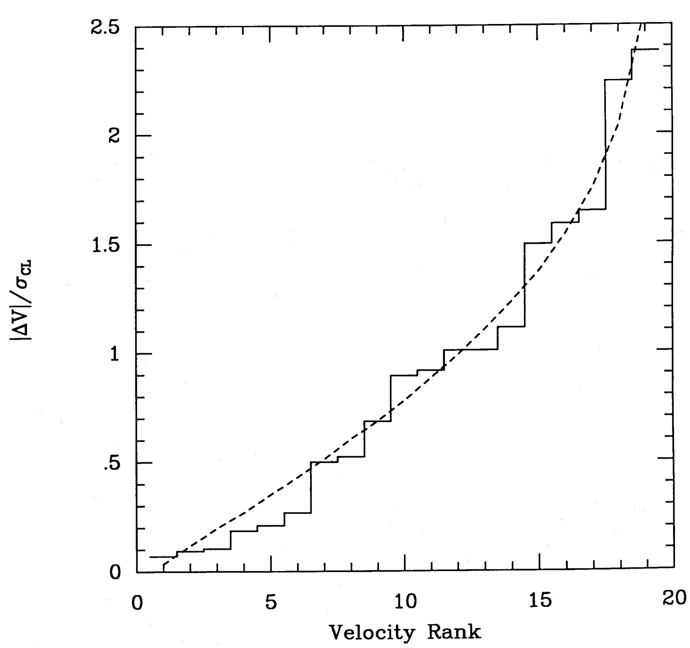

FIG. 42.—Rank-ordered radial velocity distribution (*solid line*) of all secondaries measured by Tonry (1984, 1985*a*) and Smith *et al.* (1985) that fall within the formal metric radius of $10h^{-1}$ kpc and have measured cluster dispersions, σ_{CL}, in Struble and Rood (1986). Abscissa gives the rank of the galaxy, and ordinate gives the absolute value of radial velocity of the galaxy relative to its primary, normalized by its cluster dispersion. Dashed line gives the expected velocity distribution of galaxies drawn from a Gaussian with $\sigma = 1.16\ \sigma_{CL}$.

described accurately by a Gaussian with dispersion $(1.16 \pm 0.07)\sigma_{CL}$, where σ_{CL} is the cluster velocity dispersion—the secondaries seen within the metric radius appear kinematically indistinguishable from other cluster galaxies, even though a large fraction of them may be interacting with their primaries. Further, this result is independent of cluster velocity dispersion; there is no suggestion, for example, that secondaries with relatively small radial velocity offsets occur more often in low dispersion clusters, and vice versa.

The problem remains as to what the present results say about the total luminosity, L_T, cannibalized by the average brightest cluster galaxy over the cluster lifetime. Two approaches to this problem will be attempted under the assumption that cannibalism is a steady state process that continues over the age of the cluster—alternatives to this assumption will be discussed later. The first will use a simple model of the cluster to infer L_T, given the present epoch luminosity of secondary galaxies, L_M, seen within the metric radius regardless of whether or not the secondaries are interacting with their primaries. The quantity L_T depends on both the luminosity and density distribution of galaxies within the cluster core. Over the cluster lifetime, galaxies within a luminosity-dependent infall radius, $r_i(L)$, will be pulled into a central galaxy by dynamical friction. This gives

$$L_T = 4\pi n^* L^* \int_0^\infty \left(\frac{L}{L^*}\right)^{\alpha+1} e^{-L/L^*} \frac{dL}{L^*} \int_0^{r_i(L)} r^{2-\gamma} dr \, , \quad (8)$$

assuming a Schecter (1976) luminosity function and an *initial* central density distribution that goes as $r^{-\gamma}$. For low-mass secondary galaxies in circular orbits around an isothermal primary, dynamical friction gives

$$r_i(L) = 111\left[\left(\frac{T}{5 \times 10^9 \text{ yr}}\right)\left(\frac{L}{L^*}\right) \times \left(\frac{300 \text{ km s}^{-1}}{\sigma}\right)\left(\frac{\ln \Lambda}{2}\right)\right]^{1/2} \text{kpc} \, ; \quad (9)$$

see Tremaine (1981), where T is the age of the cluster (Tremaine's value has been adopted), σ is the velocity dispersion of the primary, $\ln \Lambda$ is the standard Coulomb logarithm, and L^* corresponds to a galaxy with $M_B = -20.6$ and a mass-to-light ratio $M/L_B = 5$. The assumption of circular orbits is clearly an oversimplification; however, Tonry (1985*b*) shows that decay times are only weakly dependent on orbital eccentricity for any given semimajor axis length. Choice of the density distribution is given by the cluster profile work of Beers and Tonry (1986), who find the surface density of galaxies within the cores of clusters to fall off as r^{-1} from the center, implying $\gamma = 2$ for the spatial density profile. Cluster profiles are steeper at large radii—Dressler (1978) shows that the surface density of galaxies outside of 200 kpc can be well described by de Vaucouleurs profiles with typical $R_E \sim 4$ Mpc; however, since $r^* \equiv r_i(L^*) \ll R_E$ the present formalism is accurate over the regions of interest. The luminosity distribution of the secondary galaxies is shown in Figure 43. As can be seen, it is inconsistent with the standard $\alpha = -1.25$ Schechter (1976) luminosity distribution, and is better fitted with $\alpha = -0.75$. Although this result suggests the intriguing possibility that secondary galaxies are preferentially more luminous than a random selection of cluster galaxies, Hoessel and Schneider (1985) show that the list of multiple systems from which the present sample was drawn (Hoessel 1980) is incomplete for

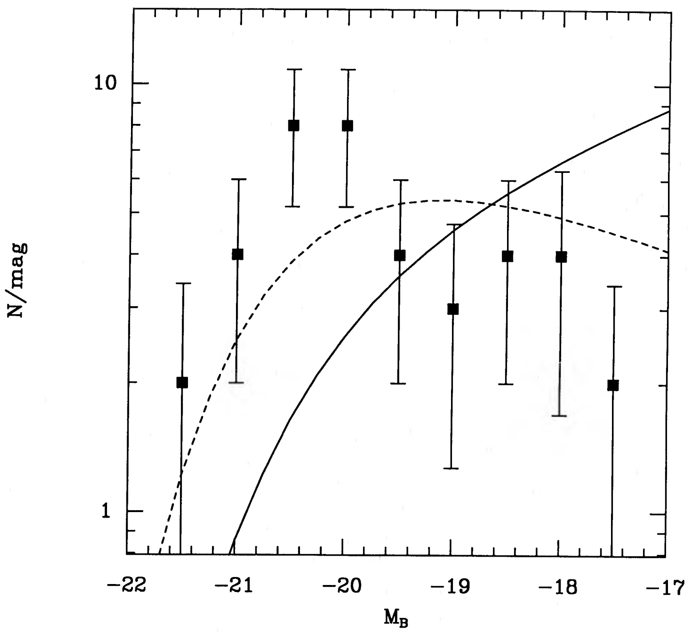

FIG. 43.—Luminosity distribution for all secondary galaxies in Table 2 and Lauer (1986) that fall within the formal metric radius of $10h^{-1}$ kpc. Galaxies are in bins 1 mag wide with centers at each half-magnitude step. Solid line is a standard Schechter (1976) with $\alpha = -1.25$ and L_* corresponding to $M_B = -20.6$, normalized to the total luminosity of the secondaries. Dashed line is a Schechter function with the same L_*, but $\alpha = -0.75$.

systems containing only faint secondaries. In the present application, however, L_T is not strongly dependent on α. The strongest contribution to L_T comes from bright galaxies whose distribution is dominated by the exponential term in the Schechter function and is only weakly dependent on α. Evaluation of equation (8) with $\alpha = -0.75$, $\gamma = -2$, and $r_i(L)$ as defined above gives $L_T \approx 11.4 n^* L^* r^*$. This choice of parameters also leads to calculation of L_M, the luminosity of galaxies visible within the metric radius at this epoch. The central surface density of galaxies visible now can be calculated from the integral along the line of sight of the initial density distribution as modified by dynamical friction. Continuity conditions and equation (9) show that the present density profile $\rho'(r)$ is related to the initial profile $\rho(r)$ by

$$\rho'(r) = \left\{1 + \left[\frac{r_i(L)}{r}\right]^2\right\}^{1/2} \rho\{[r^2 + r_i(L)^2]^{1/2}\} \, . \quad (10)$$

This implies

$$L_M = \frac{4\pi L_T}{8.8 r^*} \int_0^\infty \left(\frac{L}{L^*}\right)^{\alpha+1} e^{-L/L^*} \frac{dL}{L^*} \times \int_0^\infty \int_0^{r_m} r^{-1}[r^2 + r_i(L)^2]^{-1/2} x \, dx \, dz \, , \quad (11)$$

where r_m is the metric radius, x is the direction in the plane of the sky, z is the distance along the line of sight, and the initial $\gamma = 2$ density profile has been assumed. Evaluation of the density profile dependent part of equation (11) can be expressed as an equivalent volume, which for $r_m = 20$ kpc, and the $r_i(L)$ values of interest can be approximated as $v_e \approx 84[r^*(r_i(L)]^{2/3}$ kpc^3. Half of the integral comes within $r \sim r_m$, and it quickly converges towards its limiting value within a few more r_m from the center—again this model is not sensitive to the cluster profile at large radii. Evaluation of equation (11) with $\alpha = -0.75$ gives

$$L_T \approx 14L_M \left(\frac{r^*}{111 \text{ kpc}}\right)^{5/3} \tag{12}$$

L_M, however, is more sensitive to α than L_T; evaluation of equations (8) and (11) with $\alpha = -1.25$ leads to a coefficient in equation (12) 40% smaller than the value given. With $\alpha = -1.25$ many more low-luminosity galaxies at small radii are visible within the metric radius for the same contribution to L_T from bright galaxies compared to $\alpha = -0.75$. Results from Table 2 and Lauer (1986) give $L_M = 0.79L^*$. Comparison of the catalogs of multiple systems identified by Hoessel (1980) and Hoessel and Schneider (1985) shows that L_M averaged over all Abell clusters will be about one-third of this value or $L_M = 0.26L^*$, which from equation (12) implies $L_T \approx 4L^*$ for the average brightest galaxy in Abell clusters.

A check on L_T is provided by its relationship to the density distribution normalization n^* in equation (8). Dressler (1978), using King models to describe cluster profiles, found typical cluster core radii of $r_C \approx 0.47$ Mpc. The present power-law profile used *interior* to the core gives $n^* \approx 14 \text{ Mpc}^{-3}$ for $L_T \approx 4L^*$ at the core radius, in excellent agreement for typical galaxy densities measured there by Dressler (the comparison was made with richness class 2 clusters). In other words, the observed density of secondary galaxies within the metric radius appears to be compatible with the central power-law density profile advocated by Beers and Tonry (1986) extrapolated inward from the cluster core.

The above results suggest that cannibalism cannot form the primary galaxies, which have a typical brightness of $12L^*$ in this sample, but will cause a significant increase in their luminosities over their lifetimes (ignoring all other evolutionary effects). Of course, the calculation of L_T depends on many model parameters, and a more sophisticated analysis may arrive at a much higher value; a longer cluster age, for example, would imply more cannibalism. If anything, however, it appears that $L_T \approx 4L^*$ is more likely to be an upper limit on the amount of cannibalism. Equation (9), for example, assumes that all galaxies within the cluster core have circular velocities appropriate to the inner envelope of the central galaxy, which clearly ignores the observed high radial velocities of the secondaries. Since the effectiveness of dynamical friction decreases as V^{-2}, equation (9) may strongly overestimate $r_i(L)$ for most galaxies near the primary. Further, at radii $r \gtrsim r^*$ the mass distribution of the cluster is likely to dominate over the central galaxy, implying a higher value of σ at these radii, which again reduces the effectiveness of dynamical friction. Interestingly, the adopted density distribution does predict that half of the secondaries seen within r_m are really physically close to the primary, a result that appears to be supported by the large fraction of interacting systems of all kinematic types seen in the sample studied here. In fact, the result stated at the start of this section, that only $\sim 50\%$ of the interacting systems appear consistent with cannibalistic-type merging, suggests a correction of the L_T derived above downward by a factor of 2.

This discussion leads to the second approach of estimating L_T, which is to infer the present rate of cannibalism from the morphological analysis directly, and integrate it over the cluster lifetimes. Differentiation of equation (8) with respect to time gives

$$L_T = \left(\frac{2T}{3-\gamma}\right) \frac{dL_T}{dt}\bigg|_{t=T} ; \tag{13}$$

for $\gamma = 2$, this implies that the present cannibalism accretion rate is half the average value for the life of the cluster. The luminosity in secondaries now being cannibalized L_C is estimated from the luminosities of all secondaries not known to have high radial velocities within the five "bloated-primary" systems identified in Table 3 and that are within the metric radius. For the present sample, $L_C = 0.17L^*$; this gives the average value for all Abell clusters of $L_C = 0.058L^*$. As noted above, for the $\gamma = 2$ density profile modified by dynamical friction, the typical distance of the secondaries seen within the metric radius from their primaries is $\sim r_m$. Taking $r = 20$ kpc and the limiting infall time given by equation (10) for $L = 0.6L^*$ gives $t_i = 2.7 \times 10^8$ yr. This gives $dL_T/dt\,|_{t=T} \approx L_C/t_i$, which in turn implies $L_T \approx 2L^*$ by equation (13) and assuming $T = 5 \times 10^9$ yr.

Neither the present rate of cannibalism or the total luminosity of secondaries seen within the metric radius at this epoch imply cannibalism rates sufficient to form the brightest cluster galaxies under the simple models used here. Merritt (1985) has studied the growth of a massive centrally located cluster galaxy by cannibalism with a more sophisticated theoretical analysis, and also concludes that cannibalism will produce only modest growth, $\sim 1L^*$ over the life of the cluster. The present analysis, of course, estimates L_T from present epoch conditions under the assumption of "steady state" cannibalism. The observations cannot test the possibility raised by Merritt (1985) that first-ranked galaxies may form by the sudden collapse of a dense subcluster as appears to be happening in V Zw 311 (Schneider and Gunn 1982) and possibly in A1689 and A1934 (Schneider, Gunn, and Hoessel 1983*a*). Dressler (1984) also emphasizes observations suggesting that the formation of cD galaxies may depend more on processes occurring in small local regions of density enhhancements within a cluster rather than on steady cannibalism occurring only at the centers of rich clusters. It is noteworthy that no relationship between cluster or central galaxy type and interaction was found in the sample studied here. Of the seven cD clusters studied, for example, four showed morphological evidence for interaction with their secondaries, only one of which (A2052) is consistent with cannibalistic merging; in other words, cannibalism does not appear to be any more favored in cD galaxies compared to the rest of the primary galaxies studied.

Even if cannibalism cannot form brightest cluster galaxies, $L_T \approx 2L^*$ does represent a significant increase of their luminosities over the cluster lifetimes. The most important issue here is how this level of cannibalism will affect evolution of the luminosity within the metric radius L_γ, which is used as a standard candle for cosmological probes. Hausman and Ostriker (1978) show that L_γ grows slower than total luminosity and may even converge to a constant value if the structure of the brightest galaxy changes homologously as it cannibalizes less luminous galaxies. Although the cannibalism simulations of Duncan, Farouki, and Shapiro (1983) suggest that homologous growth does not take place in detail, simple conservation of energy argues against the metric aperture absorbing the full amount of L_T and that the global scale length of the galaxy should still grow homologously. Under the assumption of homology, Hoessel (1980) shows that L_γ for a

Hubble law brightness profile grows as

$$\frac{\Delta L_\gamma}{L_\gamma} = (1 - \alpha)\frac{L_T}{L}, \tag{14}$$

where $\alpha \equiv d \ln L_\gamma / d \ln r_m$. The primary galaxies in the present sample typically have $\alpha \approx 0.8$. With $L \approx 12L^*$ *now*, this gives $\Delta L_\gamma / L_\gamma \approx 8 \times 10^{-3}/10^9$ yr—the implied correction to q_0 measured from Hubble diagrams making use of L_γ is $\Delta q_0 \approx 0.3$ (Ostriker and Tremaine 1975). Note that this dynamical correction to q_0 is considerably smaller than the values $\Delta q_0 \approx 1.5$ derived by Hoessel (1980) and Schneider, Gunn, and Hoessel (1983*a*), who assume that all multiple systems represent cannibalistic mergers in progress. The present small dynamical value of Δq_0 needs to be confirmed with a larger sample, of course, but suggests that stellar evolution corrections, which are about $\Delta q_0 \approx -1.4$ (Tinsley and Gunn 1976), dominate the Hubble diagrams of brightest cluster galaxies.

VI. CONCLUSION

The morphology of high signal-to-noise CCD images of 16 multiple-nucleus brightest cluster galaxies has been studied using an algorithm that models images of the systems as the line-of-sight superposition of normal elliptical galaxies, which are required to have concentric elliptical isophotes, but can have otherwise arbitrary brightness, ellipticity, and position angle profiles. Eight systems are morphologically consistent with the superposition hypothesis, showing no evidence for physical interaction between their components. The residuals of the model fits to their images are flat; no faint tidal features or asymmetric shear of the component galaxies are seen. Further, the brightness profiles of the component galaxies are well described by normal $r^{1/4}$, power, or exponential laws.

In the remaining eight systems and the cD galaxy in A2199 (Lauer 1986), a variety of interaction effects between the central primary and surrounding secondary galaxies is uncovered by morphological analysis. The most striking interaction effect is asymmetrical shear of the primary galaxy, which is seen in six systems. In these systems, the nuclei are displaced from the envelope center of mass, which itself may vary as a function of radius within the envelope. Nonconcentric isophotes are not seen in isolated elliptical galaxies. A simple analysis of dynamical friction acting on a nucleus displaced from its envelope shows that asymmetric distortions are strongly damped over a crossing time, implicating a nearby secondary as the perturber. Faint tidal features or plumes are seen in five systems, which in three cases—A779, A1126, and A2199—may be consistent with dynamical friction wakes induced by the rapid passage of a secondary galaxy through the envelope of its primary. Strength of the wakes leads to estimates of the present position of the secondaries relative to their primaries. The current positions of A779B and A2199B coupled with their truncated brightness profiles imply that they are on highly radial orbits around their primaries. Lastly, abnormal brightness profiles of either the primary or secondary galaxies are seen in eight of the nine intereacting systems. Brightness profiles of three secondaries, each in a different system, are truncated at large radii, arguing for a past close encounter with their primaries. The mass-radius relationship for all secondaries shows them to be compact for their luminosities, when compared to isolated elliptical galaxies, but normal for galaxies within the cores of rich clusters (Strom and Strom 1978*a*, *b*, *c*), regardless of their association with interacting systems. In five systems, the primary appears "bloated," showing a region of excess emission over simple power or $r^{1/4}$ at radii similar to the metric radius. These systems always have a secondary with a small relative radial velocity, $|\Delta V| < 400$ km s^{-1}, while the other interacting systems have exclusively high-velocity secondaries; it is thus tempting to identify the former as sites of possible cannibalistic merging—the bloating of the primary would be a direct consequence of the secondary losing its orbital energy to the primary envelope (Hausman and Ostriker 1978).

Overall, there appears to be no kinematic difference between interacting and noninteracting multiple systems; secondaries with high and low relative radial velocities are seen in both cases. For example, in four of the interacting systems, all secondaries have $|\Delta V| > 400$ km s^{-1}, and the majority have $|\Delta V| \sim 1000$ km s^{-1}. $|\Delta V|$ in general may be related to the strength of the morphological disturbances of the interacting systems, but the only clear relationship between kinematics and interaction effects is in the bloated primary systems noted above. It is also notable that although this study suggests that some form of tidal interaction may be taking place within half of all multiple systems, the radial velocity distribution of the secondaries (Tonry 1985; Smith *et al.* 1985) is dynamically consistent with the secondaries being drawn from their cluster populations—the secondaries do not appear to form a cold subpopulation within their clusters or to be kinematically associated with their primaries. Lastly, interaction does not appear to depend on the prominence of the central galaxy or if it is a cD galaxy.

The luminosity distribution of secondary galaxies does not follow a Schechter (1976) function with standard $\alpha = -1.25$, but is better fitted with $\alpha = -0.75$; however, this result may be due to selection effects in Hoessel's (1980) catalog of multiple systems. The average total luminosity of secondary galaxies within the metric aperture for the present sample is $L_M = 0.79L^*$. If the low-velocity secondaries associated with the "bloated" primary systems are being cannibalized, then this implies that L_C, the typical total luminosity per metric aperture of galaxies now being cannibalized, is $\sim 25\%$ of L_M, or $L_C = 0.17L^*$. These imply average values for all first-ranked galaxies in Abell clusters of $L_M = 0.26L^*$ and $L_C = 0.058L^*$, which can be viewed as present-epoch "zero-points" for evolutionary modeling of the structure of first-ranked galaxies.

Although detailed modeling of the growth of a central galaxy in a cluster is beyond the scope of this paper, both L_M and L_C can be used in simple models to calculate the total luminosity, L_T, cannibalized by a central galaxy over the cluster lifetime. The present value of L_M represents the integral of the cluster density profile along the line of sight over the metric aperture at this epoch, and therefore implies a value of L_T for any given form of an initial cluster density profile. Likewise, L_C gives an estimate of the current rate of cannibalism, which can be integrated to the cluster lifetime to get a separate measure of L_T. Both methods give $L_T \approx 2L^*$ over 5×10^9 yr, under the assumption of "steady state" cannibalism in a cluster with an initial r^{-2} density profile. In this case, cannibalism is insufficient to form the primary galaxies, which typically have $L \sim 12L^*$, but will still produce a significant evolutionary increase in the metric luminosities. Under the assumption that the primary galaxies grow homologously, the present value of L_T implies a dynamical correction of $\Delta q_0 \approx$

0.3 to q_0 measured from Hubble diagrams of brightest cluster galaxies.

I wish to thank Jim Gunn for the images and useful discussions. I am also grateful to Jerry Ostriker, Scott Tremaine, and Barbara Ryden for useful discussions. This work was supported by NSF grant AST84-20352 and NASA grant NAS5-25451.

REFERENCES

Anguilar, L. A., and White, S. D. M. 1986, *Ap. J.*, **307**, 97.
Beers, T. C., and Tonry, J. L. 1986, *Ap. J.*, **300**, 557.
Borne, K. D. 1984, *Ap. J.*, **287**, 503.
Burstein, D., and Heiles, C. E. 1984, *Ap. J. Suppl.*, **54**, 33.
Chandrasekhar, S. 1942, *Principles of Stellar Dynamics* (Chicago: University of Chicago Press).
de Vaucouleurs, G., de Vaucouleurs, A., and Corwin, H. G. 1976, *Second Reference Catalogue of Bright Galaxies* (Austin: University of Texas Press).
Dressler, A. 1978, *Ap. J.*, **226**, 55.
———. 1984, *Ann. Rev. Astr. Ap.*, **22**, 185.
Duncan, M. J., Farouki, R. T., and Shapiro, S. L. 1983, *Ap. J.*, **271**, 22.
Gunn, J. E., *et al.* 1987, preprint.
Hausman, M. A., and Ostriker, J. P. 1978, *Ap. J.*, **224**, 300.
Hoessel, J. G. 1980, *Ap. J.*, **241**, 493.
Hoessel, J. G., Borne, K. D., and Schneider, D. P. 1985, *Ap. J.*, **293**, 94.
Hoessel, J. G., and Schneider, D. P. 1985, *A.J.*, **90**, 1648.
Jenner, D. C. 1974, *Ap. J.*, **191**, 55.
Kormendy, J. 1977, *Ap. J.*, **218**, 333.
Lauer, T. R. 1985, *M.N.R.A.S.*, **216**, 429.
———. 1986, *Ap. J.*, **311**, 34.
Lauer, T. R., Stover, R. J., and Terndrup, D. M. 1983, *Lick Obs. Tech. Rep.*, No. 34.
Leir, A. A., and van den Bergh, S. 1977, *Ap. J. Suppl.*, **34**, 381.
Merritt, D. 1984, *Ap. J. (Letters)*, **280**, L5.
———. 1985, *Ap. J.*, **289**, 18.
Miller, R. H. 1986, *Astr. Ap.*, **167**, 41.
Mulder, W. A. 1983, *Astr. Ap.*, **117**, 9.
Ostriker, J. P., and Tremaine, S. D. 1975, *Ap. J. (Letters)*, **202**, L113.
Owen, F. N., O'Dea, C. P., Inoue, M., and Eilek, J. A. 1985, *Ap. J. (Letters)*, **294**, L85.
Schechter, P. L. 1976, *Ap. J.*, **203**, 297.
Schneider, D. P., and Gunn, J. E. 1982, *Ap. J.*, **263**, 14.
Schneider, D. P., Gunn, J. E., and Hoessel, J. G. 1983*a*, *Ap. J.*, **268**, 476.
———. 1983*b*, *Ap. J.*, **264**, 337.
Smith, R. M., Efstathiou, G., Ellis, R. S., Frenk, C. S., and Valentijn, E. A. 1985, *M.N.R.A.S.*, **216**, 71P.
Strom, K. E., and Strom, S. E. 1978*a*, *A.J.*, **83**, 1293.
———. 1978*b*, *A.J.*, **83**, 73.
———. 1978*c*, *A.J.*, **83**, 732.
Struble, M. F., and Rood, H. J. 1982, *A.J.*, **87**, 7.
———. 1987, *Ap. J. Suppl.*, **63**, 543.
Tinsley, B. M., and Gunn, J. E. 1976, *Ap. J.*, **203**, 52.
Tonry, J. T. 1984, *Ap. J.*, **279**, 13.
———. 1985*a*, *A.J.*, **90**, 2431.
———. 1985*b*, *Ap. J.*, **291**, 45.
Tremaine, S. D. 1981, in *The Structure and Evolution of Normal Galaxies*, ed. S. M. Fall and D. Lynden-Bell (Cambridge: Cambridge University Press), p. 67.
Weinberg, M. D. 1986, *Ap. J.*, **300**, 93.

TOD R. LAUER: Princeton University Observatory, Peyton Hall, Princeton, NJ 08544